THE UNIVERSITY OF MICHIGAN
ANN ARBOR, MICHIGAN

INTERIM SCIENTIFIC REPORT NO. 3

FOR

SOLID-STATE MICROWAVE RESEARCH

This report covers the period April 1, 1964 to July 1, 1964

Electron Physics Laboratory
Department of Electrical Engineering

By: D. C. Hanson
J. E. King
J. E. Rowe
C. Yeh

Approved by: J. E. Rowe
J. E. Rowe, Director
Electron Physics Laboratory

Project 06031

Contract No. AF 33(657)-11587
Electronic Technology Division
Air Force Avionics Laboratory
Research and Technology Division
Air Force Systems Command
Wright-Patterson Air Force Base, Ohio

August, 1964

ABSTRACT

The characteristics of phonon interactions in solids are discussed in relation to possible parametric interactions in vanadium doped cadmium sulfide. The energy eigenvalues for cadium sulfide are plotted and discussed.

A theory of operation is proposed to explain the "Gunn effect" in bulk semiconductors. Experimental evidence is given for GaAs indicating radiation output in the wavelength region from 300-3000 microns.

The ω-β diagram for the longitudinal acoustic-wave amplifier is presented and discussed. The deformation potential acoustic-wave amplifier is analyzed. Thin film transducers are discussed.

TABLE OF CONTENTS

LIST OF ILLUSTRATIONS

LIST OF TABLES

PERSONNEL

Scientific and Engineering Personnel		Time Worked in Man Months*
J. Rowe	Professors of Electrical Engineering	.10
C. Yeh		.30
W. Rensel	Assistant Research Engineer	.37
D. Hanson	Research Assistants	2.16
J. King		3.02
R. Maire		.37
Service Personnel		5.95

* Time Worked is based on 172 hours per month.

INTERIM SCIENTIFIC REPORT NO. 3

FOR

SOLID-STATE MICROWAVE RESEARCH

1. General Introduction (J. E. Rowe)

The purpose of this research study is to investigate the general characteristics of high-frequency (microwave) interactions in bulk semiconductors. The program is a general one concerned with the generation, amplification and detection of coherent electromagnetic energy in the centimeter through optical regions of the electromagnetic spectrum.

Although the general areas of study under this program cover a wide range of topics, the initial studies have been specialized to the following areas:

a. Phonon interactions in solid-state materials.

b. Generation in and radiation from solids.

c. Acoustic-wave interactions, including both longitudinal and shear mode excitations.

As each of the investigations progress it is planned that specific experiments will be designed to check the theoretical results. Each of the above topics is discussed in detail in the following sections of this report.

2. Phonon Interaction in Solids (J. E. King)

2.1 Introduction. During the past period work was continued on the ruby rod. The rod was operated at liquid nitrogen temperature. In addition a second transducer was bonded to the rod to allow two frequency operation. After investigating propagation in ruby it was felt that other materials would be much more suited to parametric interaction.

Early in the period covered by this report a sample of cadmium sulfide doped with vanadium was obtained. In order to investigate this

further and to determine the energy level configuration, electron paramagnetic resonance has been attempted. So far the spectrometer has given inconsistent results. Considerable effort has been put into improving the sensitivity of the spectrometer. Some preliminary energy levels have been calculated from the spin-Hamiltonian. These will be used to check against experimental results.

Several articles have been reviewed concerning ultrasonic spin resonance[1,2,3,4] and also nonlinear acoustic interaction[5] and parametric amplification[6].

2.2 Literature Review. The work of Browne and Dobrov[3] using ruby is very interesting as they have correlated phonon absorption and spin lattice relaxation times. In addition they have several absorption curves obtained using their spectrometer. It appears as if the spectrometer they use is too complex to duplicate at this time. This instrument is designed to integrate pulses and to display this as an absorption signal. In this manner they obtain the absorption line shape where in electron paramagnetic resonance the derivative of the absorption curve is normally displayed.

---

1. Shiren, N. S., "Comparison of Ultrasonic Spin Resonance Measurements with Paramagnetic Relaxation Theory", Proc. of the International Conference on Magnetic and Electronic Resonance and Relaxation, Eindhoven, Holland, pp. 114-122; 1962.

2. Shiren, N. S., "Dipolar Broadening from Pulse Velocity in Ultrasonic Spin Resonance", Paramagnetic Resonance, Academic Press, New York, pp. 482-485; 1963.

3. Browne, M. E. and Dobrov, W. I., "Magnetic Resonance Absorption of Hypersonic Waves in Paramagnetic Crystals", Jour. of the Phys. Soc. of Japan, vol. 17, supplement B-I, pp. 469-471; 1962.

4. Dobrov, W. I. and Browne, M. E., "Low Temperature Relaxation in Ruby from Microwave Acoustic Measurement", Paramagnetic Resonance, Academic Press, New York, pp. 447-455; 1963.

5. Shiren, N. S., "Nonlinear Acoustic Interaction in MgO at 9 Gc/sec", Phys. Rev. Letters, vol. 11, No. 1, pp. 3-6; 1 July 1963.

6. Shiren, N. S., "Ultrasonic Traveling-Wave Parametric Amplification in MgO^{1}", Appl. Phys. Letters, vol. 4, No. 4, pp. 82-85; 15 February 1964.

Shiren's[1,2] work shows excellent agreement between ultrasonic measurements and static stress measurements for the fourth rank spin-phonon coupling tensor G. Using this data he is able to calculate relaxation times in reasonable agreement with measured values.

Two important articles by Shiren[5,6] were reviewed. In the first of these, he reports a strong nonlinear interaction which is characterized by an increased absorption of the signal. This absorption is power dependent and can result in as much as an increase of 65 to 70 percent in the absorption. This nonlinear effect is the result of anharmonic restoring forces between adjacent atoms. Shiren showed that the nonlinear effect was not due to impurities in the crystal but only due to the anharmonic restoring forces. He attributed the interaction to a three-phonon process, i.e., a signal, a pump and an idler. For the nonlinear effect to occur the waves must satisfy the following parametric equations:

$$\omega_p = \omega_s + \omega_i \quad ,$$

$$\beta_p = \beta_s + \beta_i \quad . \tag{2.1}$$

Thus by using phonon paramagnetic resonance Shiren was able to mismatch the phase constants so that

$$\beta_p \neq \beta_s + \beta_i$$

and thus eliminate the nonlinear interaction. The mechanism for doing this is the same as outlined in an earlier progress report. The phonon paramagnetic resonance introduces a slowing of the group velocity and also a change in the phase velocity as the frequency of the phonon wave

passes through a resonance. Consequently it is possible to mismatch the phase constants by turning the resonance to one of the frequencies involved.

There was no observed change in nonlinear effect over a temperature range from 1.6°K to 4.2°K. The nonlinearity was also not affected by the concentration of impurities. This further substantiates the belief that it is a property of the lattice and not of the paramagnetic ions.

In the second paper Shiren reports gain due to parametric amplification. He achieved gain by tuning the phonon paramagnetic resonance to simultaneously mismatch the pump plus signal frequency and twice the pump frequency which was made possible since the sample contained two different impurities, nickel and iron. These ions have different g-values and so split at different rates in a magnetic field. The crystal MgO is cubic so that there is no zero field splitting and thus, by correct choice of frequencies, it is possible to have the s + p and 2p frequencies resonant at the same magnetic field in the two different spin systems.

These two papers offer experimental evidence for traveling-wave parametric amplification of acoustic waves. One of the difficulties of Shiren's techniques is that the ω-β diagram is linear out to the frequency s + p. This means that any frequencies less than the pump frequency will satisfy the parametric interaction conditions. Thus it would seem possible that a large part of the nonlinear interaction is wasted in "noise" caused by all other undesired frequencies. Gain is thus achieved for only those modes in which the upper side band is tuned out, thus converting additional power into the signal frequencies. Because of this the system proposed in our previous work should be considerably better. By using several tunable resonances it would be possible to eliminate the upper side band and, in addition, to have the parametric conditions satisfied for only the particular pump and signal frequencies.

This would allow considerably more power to be transferred into the signal frequency.

A second difficulty is that by using a cubic crystal there is little tuning of the energy levels since they split linearly with magnetic field. Also because of the requirements of eliminating higher harmonics of the pump and signal frequencies it is desirable to have both resonants at the same magnetic field value. This requirement fixes the frequency ratio for pump and signal in a cubic crystal since two separate spin systems are required, each with its own g-value. In a noncubic crystal such as cadmium sulfide, this problem is eliminated since the energy levels vary with angle from the c-axis. Thus it would appear possible to satisfy the simultaneous resonance condition for perhaps several different signal frequencies.

2.3 Ruby Investigation. Leads were effectively attached to the quartz transducers for operation at liquid nitrogen temperature using indium solder. A noticeable improvement in the echo pattern has been observed when operating at 77°K. This is attributed to the improvement in the mechanical bond between transducer and rod. Using this apparatus echoes have been seen as high as 892 mc. This has been achieved using a configuration similar to that illustrated in Interim Scientific Report No. 1; Fig. 2.3, p. 28. For this application resonant transducers with gold plating on each side have been bonded to each end of the ruby rod. These transducers are resonant at 17.5 mc and 10.5 mc respectively, i.e., in the ratio 5:3. Thus every fifth harmonic of the 10.5 mc transducer corresponds to every third harmonic of the 17.5 mc transducer. Thus it is possible to obtain transmission at the following frequencies (only odd harmonics resonate):

Table 2.1

Transducer Eigenfrequencies

f (mc)	Harmonic No. of 17.5 mc Transducer	Harmonic No. of 10.5 mc Transducer
52.5	3	5
157.5	9	15
262.5	15	25
367.5	21	35
472.5	27	45
577.5	33	55
682.5	39	65
787.5	45	75
892.5	51	85

One can see that 892.5 mc operation occurs at a very high harmonic of the fundamental resonance. This means that any imperfections in parallism and surface preparation is most noticeable. In addition the attenuation constant of the material is getting larger at the higher frequencies. Consequently it is more difficult to see echoes at the very high frequencies. Because of these effects only one echo was observed at 892.5 mc and it was quite weak.

The use of two resonant transducers also allows multiple frequency operation. Consequently effects were investigated using a very high power pump at approximately twice the frequency of the smaller signal. The pump was square wave modulated and the signal was pulsed. This allowed a resonant build-up of pump power in the rod and then application of the signal pulse. The purpose of this experiment is to determine if there is any nonlinear pumping action within the

crystal due to anharmonic coupling forces between atoms in the lattice. So far no effect has been observed. Experiments have been carried on with a pump frequency of 402.5 mc and a signal of 201 mc.

As mentioned in earlier reports, the phonon absorption coefficient for ruby is very small and consequently any phase change introduced in the ω-β diagram would be very small. Although the nonlinear interaction in the crystal may be present, it is felt that the tuning required for successful amplifier operation could not be achieved because of the small change in phase constant. Thus further investigation of ruby as a traveling-wave parametric acoustic amplifier will be dropped. The future work will be done on the vanadium doped cadmium sulfide since the absorption coefficient should be many orders of magnitude larger.

2.4 EPR Spectrometer. Considerable effort has been put into improving a spectrometer. One of the earlier configurations utilized a traveling-wave amplifier and a transmission cavity to selectively return the signal to the amplifier so that oscillation occurred. The sample is then placed in the cavity. The advantage to this scheme is automatic frequency stabilization due to the fact that the cavity determines the frequency of oscillation. As the frequency of the cavity shifts due to changes in the dielectric constant of the sample, the oscillation frequency automatically follows. The disadvantage is that operation is limited to the fundamental frequency of the transmission cavity. It is necessary to investigate the spectrum over a range of 4 to 10 Gc due to the splitting of the energy levels. This would mean a number of different cavities as well as traveling-wave amplifiers. Oscillations at other frequencies cause noise so that only the fundamental cavity frequency should be present.

In order to satisfy the requirements a coaxial system seems most appropriate. However, the lack of a coaxial equivalent of the waveguide hybrid tee makes coaxial systems very difficult. Several different configurations have been tried with the results to date being erratic. A coaxial cavity, tunable from 1 to 10 Gc, has been built. Using this cavity it has been possible to operate over a wide frequency range with good coupling to the cavity.

A modulator and phase sensitive detector were ordered some time ago. Unfortunately the modulator and phase sensitive detector have not arrived. However, using a laboratory-built detector, efforts have been made to increase the sensitivity. The sensitivity of the apparatus undergoes daily variations so that no consistent results have been obtained. Considerable effort has been put into determining the cause of these variations with no result. The apparatus being used is very sensitive to changes in the reflection coefficient of the cavity. Thus any minute disturbance of the frequency of the signal generator due to line variations etc. is greatly amplified. In addition vibrations of the cavity also cause some variation. When operating at liquid nitrogen, bubbling causes severe problems.

The spectrometer has been checked out using a small quantity of DPPH, an isotropic, $g = 2$ line. The spectrometer is adjusted to this line and then the vanadium spectrum is investigated. So far a small chip of ruby has been observed as well as a small piece of MgO with manganese and chromium dopants. When the spectrometer can consistently reproduce the spectrum due to the small piece of ruby, it should be sensitive enough to observe the CdS:V lines.

2.5 Cadmium Sulfide:Vanadium Energy Eigenvalues. The energy eigenvalues are obtained by finding the matrix elements of the Hamiltonian

and then finding the characteristic values. The eigenvectors could then be found which would indicate the admixture of the pure spin states in each eigenvector. To be precise, the eigenvalues should be obtained for each of the 24 energy levels, three fine lines each divided into eight hyperfine lines due to the vanadium nuclear spin. The spectrum is further complicated by two inequivalent spin sites. The Hamiltonian is given by

$$\mathcal{H} = \beta [g_{\parallel} J_z H_z + g_{\perp} (J_x H_x + J_y H_y)] + D J_z^2$$

$$+ \frac{a}{6} [J_\xi^4 + J_\eta^4 + J_\zeta^4] + \frac{F}{180} [35 J_z^4 - 30 J(J+1) J_z^2 + 25 J_z^2]$$

$$+ A J_z I_z + B (J_x I_x + J_y I_y) \quad . \qquad (2.2)$$

The ξ, η, ζ axes are given so that the body diagonal of the cube formed by the ξ, η, ζ unit vectors lies along the z-axis. It is possible to show that for the appropriate orientation of the $\xi\eta\zeta$ axis and since $J = 1$ the terms in a and F do not contribute. Also $g_{\parallel} \approx g_{\perp}$ and $A \approx B$ so that the Hamiltonian can be approximately reduced to

$$\mathcal{H} = g\beta\, J \cdot H + D J_z^2 + A J \cdot I \quad . \qquad (2.3)$$

To simplify the results, assume $A = 0$. This gives a 3 x 3 matrix which can be solved for the energy-eigenvalues. The spin state $J = 1$ is represented by the eigenstate $|1>$, $J = 0$ by $|0>$ and $J = -1$ by $|-1>$. The matrix elements are then given by

Table 2.2

Hamiltonian Matrix Elements

	$\|+1\rangle$	$\|0\rangle$	$\|-1\rangle$
$\langle +1\|$	$D + g\beta H \cos\theta$	$\frac{1}{\sqrt{2}} g\beta H \sin\theta\, e^{i\psi}$	0
$\langle 0\|$	$\frac{1}{\sqrt{2}} g\beta H \sin\theta\, e^{-i\psi}$	0	$\frac{1}{\sqrt{2}} g\beta H \sin\theta\, e^{i\psi}$
$\langle -1\|$	0	$\frac{1}{\sqrt{2}} g\beta H \sin\theta\, e^{-i\psi}$	$D - g\beta H \cos\theta$

where θ is the polar angle from the z-axis and ψ is the angle measured in the x-y plane from the x-axis.

Diagonalizing this matrix and solving gives the energy levels of Fig. 2.1 for angles of $\theta = 0°$, $\cos^{-1} 1/\sqrt{3}$ and $90°$.

With $A \neq 0$ the matrix becomes considerably more complicated and expands to a 24 x 24 matrix. In general there is no simplification that results in a reduction of the matrix except by setting $\theta = 0°$. This eliminates off diagonal terms due to electron spin but does not affect the terms due to nuclear spin-electron spin interaction. At $\theta = 0°$ the matrix breaks up into six 3 x 3 submatrices, two 2 x 2 and two 1 x 1 matrices. Hence it is possible to calculate the energy eigenvalues at 0°. If a spin eigenstate is denoted by $|M, m\rangle$, where M is the electronic spin quantum number and m the nuclear spin quantum number and the matrix elements between these states at 0° are evaluated, it is found that the submatrices involve admixtures of the following states:

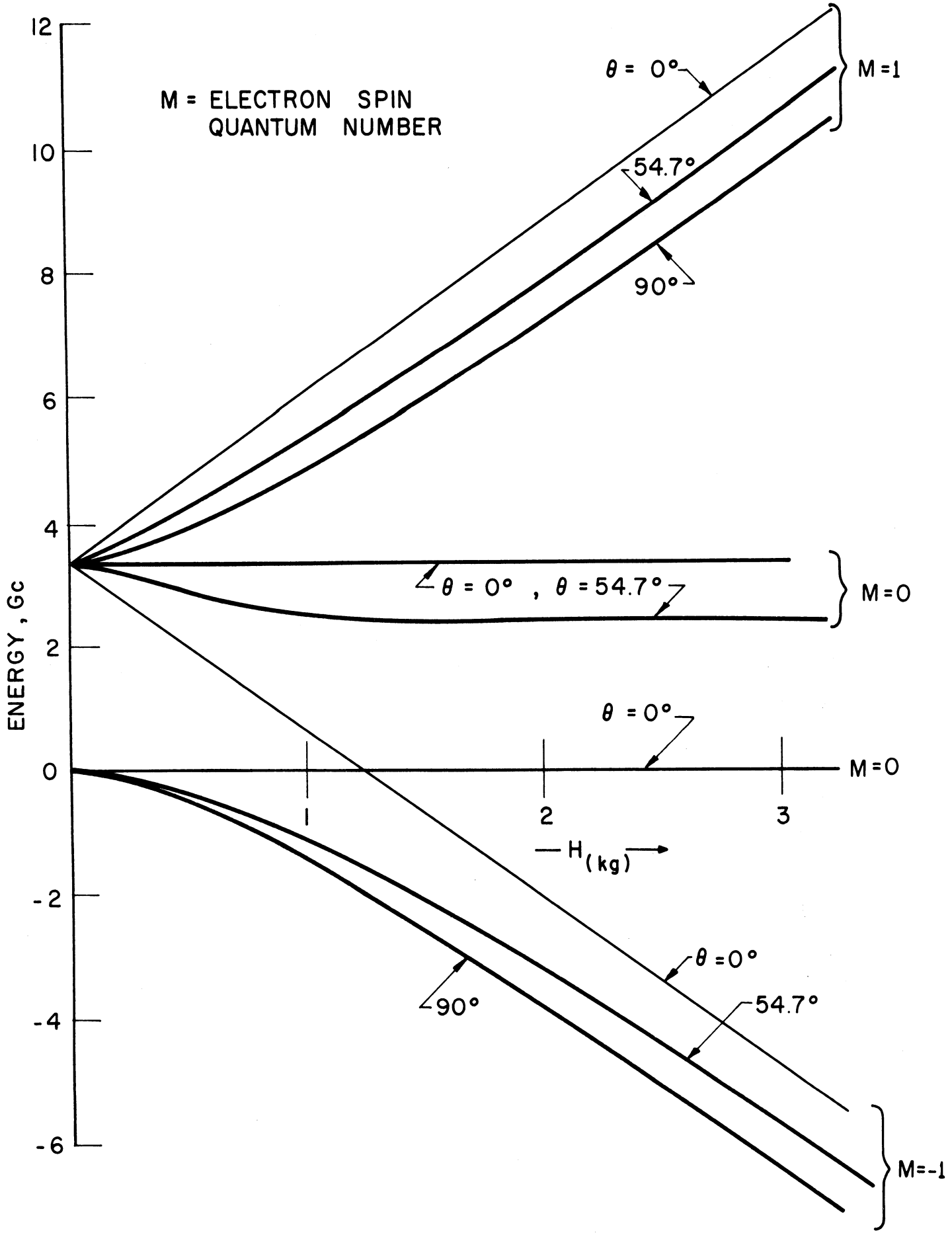

FIG. 2.1 ENERGY EIGENVALUES AS A FUNCTION OF ANGLE, A = 0.

$|1, 7/2>$

$|0, 7/2>$ and $|1, 5/2>$

$|-1, 7/2>$, $|0, 5/2>$, and $|1, 3/2>$

$|-1, 5/2>$, $|0, 3/2>$, and $|1, 1/2>$

$|-1, 3/2>$, $|0, 1/2>$, and $|1, -1/2>$

$|-1, 1/2>$, $|0, -1/2>$, and $|1, -3/2>$

$|-1, -1/2>$, $|0, -3/2>$, and $|1, -5/2>$

$|-1, -3/2>$, $|0, -5/2>$, and $|1, -7/2>$

$|-1, -5/2>$, and $|0, -7/2>$

$|-1, -7/2>$

This shows the six 3 x 3 submatrices, the two 2 x 2's and the two unperturbed states. Some of the submatrices have been diagonalized and the energy eigenvalues were determined. Those chosen were the two unperturbed levels, the two 2 x 2's and the first and last 3 x 3 since they differed only in the signs of some of the terms. The eigenvalues are determined by solving $W = D + (7/2)\,A + g\beta H$, $W = D + (7/2)\,A - g\beta H$

$$W^2 - [g\beta H + D + (5/2)\,A]\,W - (7/2)\,A^2 = 0 \ ,$$

$$W^2 - [-g\beta H + D + (5/2)\,A]\,W - (7/2)\,A^2 = 0 \ ,$$

$$[-g\beta H + D - (7/2)\,A - W]\,[W^2 - \{g\beta H + D + (3/2)\,A\}\,W - 6A^2]$$

$$- (7/2)\,A^2\,[g\beta H + D + (3/2)\,A - W] = 0$$

and

$$[g\beta H + D - (7/2)\,A - W]\,[W^2 - \{-g\beta H + D + (3/2)\,A\}\,W - 6A^2]$$

$$- (7/2)\,A^2\,[-g\beta H + D + (3/2)\,A - W] = 0 \ ,$$

and using D = 0.1130 cm^{-1} and

A = 0.0064 cm^{-1}.

The curves of Fig. 2.2 are then obtained. Note that although A is more than one order of magnitude smaller than D the curves are drastically affected for magnetic field less than 1 kg. Also it is possible to get transitions between states which are mixed.

2.6 Program for the Next Quarter. The spectrometer will be improved to give consistent results. The arrival of the modulator and detector should greatly improve results. After checking energy levels, phonon paramagnetic resonance will be done and then parametric operation will be attempted.

3. Radiation from Solids (D. C. Hanson)

3.1 Introduction. During the early part of this past quarter, before the GaAs planar structures arrived from Texas Instruments, effort was directed toward understanding and developing an impurity scattering theory including the mechanism of generation of radiation. This theory should include coupling of this internally generated radiation to the polar optical phonon vibrational modes in such III-V compounds as GaAs. Close coupling and nonlinear interaction would presumably allow for frequency conversion of internally generated radiation since theory[1] indicates (as presented in Interim Scientific Report No. 1) that stimulated emission of Bremsstrahlung radiation from impurity scattering has a strong f^5 power relationship, thus making watts of power available only at frequencies near and above 1000 Gc.

After the GaAs planar structures arrived an experimental program was begun. Initial effort was directed toward a superior mounting scheme

---

1. Marcuse, D., "Stimulated Emission of Bremsstrahlung", BSTJ, vol. XLI, No. 5, pp. 1557-1571; September, 1962.

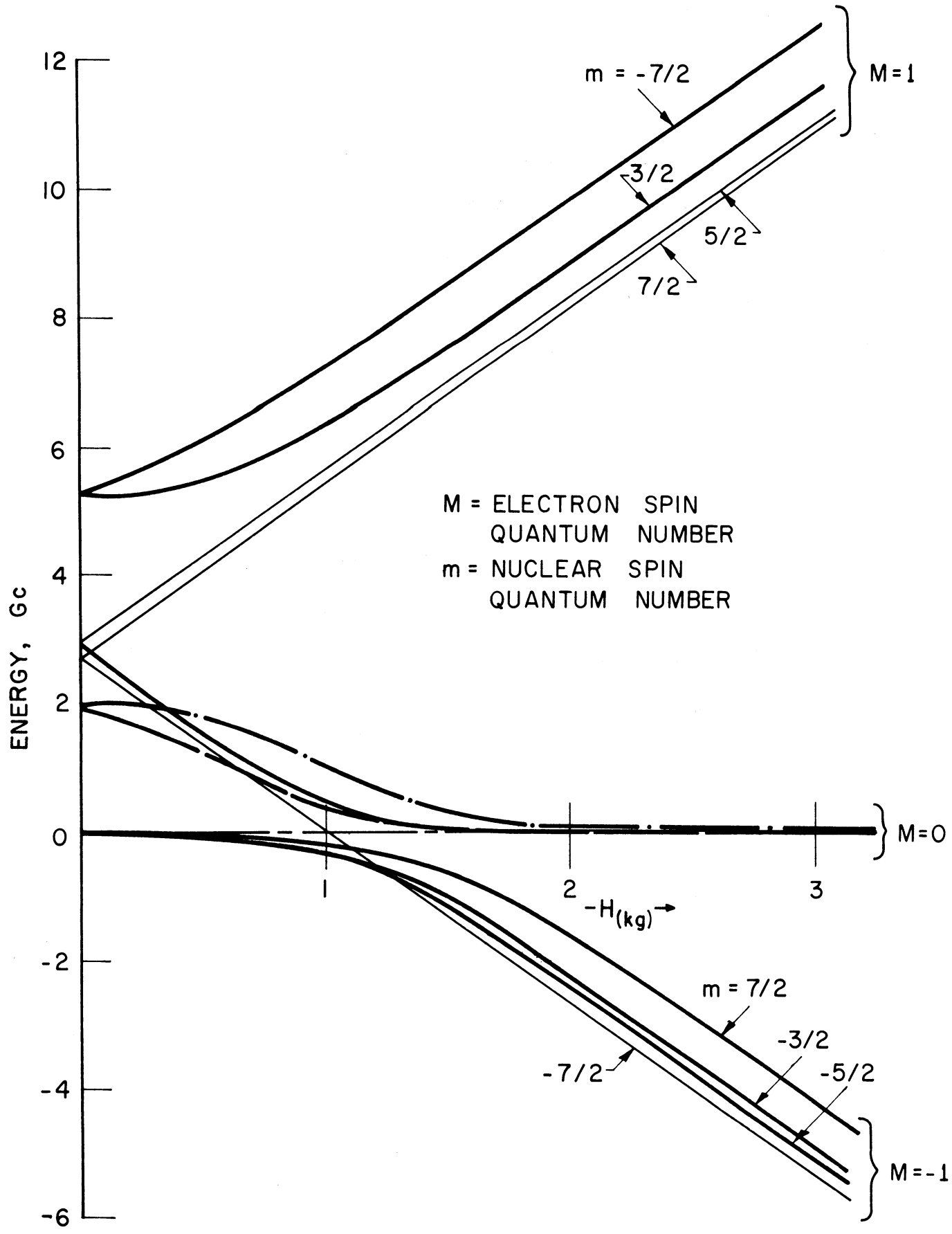

FIG. 2.2 TWELVE OF THE TWENTY-FOUR ENERGY EIGENVALUES FOR $\theta = 0°$, $A \neq 0$.

which would provide very low resistance ohmic contacts and also good heat sink capability. With this achieved, radiation was detected above 50 Gc using a cutoff waveguide coupling approach and a Golay cell detector as described in the experimental section of this report. Subsequently, using a Perkin-Elmer far infrared spectrometer it was established that the detected radiation is indeed concentrated in the far infrared region, thus lending confirmation to the theory of stimulated emission of Bremsstrahlung radiation from impurity scattering. Recorder plots show what is believed to be the first significant far infrared radiation detected from bulk semiconductors due to hot carrier phenomena.

3.2 Theory. Impurity scattering theory is not well understood, as pointed out in Interim Scientific Report No. 2, since it has been necessary to postulate energy losses several times larger than that of the assumed models to account for observed mobilities and considerable variations have been observed in impurity scattering dominated mobility under supposedly similar conditions. Herring[2] and Lax[3] have pointed out the inherent limitations of the usual Boltzmann transport equation,

$$\left(\frac{\partial f}{\partial t}\right)_{\text{field}} + \left(\frac{\partial f}{\partial t}\right)_{\text{collisions}} = 0 \ ,$$

which has been used in impurity scattering theory. The most severe limitation is that a random phase approximation is made after each scattering event and thus all phase information is lost in scattering and the density matrix describing the system is considered to be diagonal at all times. This is a particularly severe limitation if

---

2. Herring, C., "Transport", Jour. Phys. Chem. Solids, vol. 8, pp. 543-549; January, 1959.

3. Lax, M., "Generalized Mobility Theory", Phys. Rev., vol. 109, pp. 1921-1926; March 15, 1958.

the average time between collisions is not long as is the case in high current density experiments with impurity concentrations of about $10^{17}/cm^3$ in GaAs.

Since this random phase approximation has invariably been made in previous impurity scattering theories, it is not unreasonable that the significance of selective electron scattering in the forward direction with generation of Bremsstrahlung radiation[1] has thus far been overlooked in transport theory. Other aspects of this theory have been discussed in Quarterly Progress Reports No. 1 and No. 2.

It is apparent from a search of the literature that a transport and radiation theory should incorporate the work of Kohn and Luttinger[4,5]. In these two definitive papers on the quantum theory of electrical transport, the entire transport density matrix is developed, thus including phase information in the transport equations. The model consists of Bloch electrons being scattered by "random" rigid impurity centers and it is shown that the familiar Boltzmann transport equation is only a valid approximation in the limiting case of very weak and very dilute scatterers.

A recent more detailed report by Gunn[6] states the very interesting experimental result (which was not discussed at all) that in no case have ohmic-n-ohmic structures failed to show instabilities in current, whereas ohmic-p-ohmic structures of GaAs have never shown instabilities up to fields of 4×10^4 volts/cm. If differences in the contacts can be neglected it would seem that this should provide some valuable insight

---

4. Kohn, W. and Luttinger, J. M., "Quantum Theory of Electrical Transport Phenomena", Phys. Rev., vol. 108, No. 3, pp. 590-611; November, 1957.

5. Kohn. W. and Luttinger, J. M., "Quantum Theory of Electrical Transport Phenomena II", Phys. Rev., vol. 109, No. 6, pp. 1892-1909; March 15, 1958.

6. Gunn, J. B., "Instabilities of Current in III-V Semiconductors", IBM Jour., pp. 141-159; April, 1954.

into the radiation mechanism and will be discussed here based on the information presented in Quarterly Progress Report No. 2.

Since electrons are the charge carriers for both the n-type and p-type structures with ohmic contracts it would apprear that the main difference between the consistent observation of current instabilities in n-type GaAs and the complete absence of current instabilities in p-type GaAs is due to the fact that in relatively uncompensated n-type material there is a large majority of fixed, positively charged donors, whereas in p-type material fixed, negatively charged acceptors predominate. The former gives rise to attractive scattering of electrons while the latter produces repulsive scattering. The paper by Sclar[7] (discussed in Quarterly Progress Report No. 2) shows that only in the former case does resonant scattering occur with electrons scattered selectively in the forward direction (i.e., the Ramsauer effect) thus satisfying the conditions of Marcuse's theory of radiation[1]. This appears to be a highly significant observation to support the theory that impurity scattering generation of Bremsstrahlung radiation is responsible for the observed[6] radiation.

3.3 Experimental Program.

3.3.1 GaAs Structures. With the arrival of GaAs structures from Texas Instruments with dimensions of 0.080 in. x 0.080 in. x 0.004 in., initial effort was devoted to obtaining a suitable mounting procedure to a heat sink to obtain very low resistance ohmic contacts. The GaAs structures in the initial experiments were grown by the Czochrolski process and doped with tellurium (an n-type dopant) to a concentration of $10^{17}/cm^3$. The bulk resistivity is about 0.01 ohm-cm and mobility of

---

7. Sclar, N., "Ionized Impurity Scattering in Nondegenerate Semiconductors", Phys. Rev., vol. 104, pp. 1548-1561; December 15, 1956.

approximately 4000 cm^2/volt-sec. The two large area surfaces are rhodium plated to allow direct soldering of the GaAs structures to a heat sink.

The initial group of structures had to be returned to Texas Instruments since the low melting point (125°C) InSn solder would not adhere to one surface of the structure which was not initially coated with solder due to a surface condition. However, with the new structures, the total resistance of a bulk specimen 0.004 in. x 0.050 in. x 0.050 in. is approximately 0.030 ohms. Since the calculated bulk resistance is 0.003 ohm, this indicates that very good ohmic contacts exist.

The entire semiconductor-heat sink structure is made by precoating the square contact surface of a brass heat sink with a thin coating of solder, positioning the precoated GaAs structure on the heat sink and then placing a 0.003 in. x 0.080 in. x 0.080 in. gold foil square, which has been precoated with In-Sn solder on its bottom side, above the GaAs structure. The entire assembly is then placed in a jig and moderate pressure is applied from the top by a coaxial bellows at room temperature. As the assembly is slowly heated to above 125° the GaAs structure is securely soldered between the heat sink and gold cap and the excess solder is forced out automatically by the bellows. The soldered structure is then filed or ground to the desired square size, thus removing solder from the surface and presenting a clean GaAs surface for radiation studies. In actual electrical operation pressure contact is made to the gold cap with a beryllium copper c-spring at the end of a coaxial center conductor. To this point it has not been possible to make structures which are less than 0.035 in. square by this process due to the forces which occur during the last mechanical operation.

As described in the next section, this mounting and heat sink arrangement has allowed continuous operation for hours at a time using

10-15 amps of current chopped at a 13 cps rate with a 50 percent duty cycle. No noticeable deterioration has occurred in the radiation performance or in the structure, thus continuous operation at this current density appears to be no problem since structure heating should have equalized during the 77 msec half period of the current pulse.

3.3.2 Direct Detection Procedure. Initial consideration was given to obtaining a suitable detector in the 100 μ to 1000 μ region. A mount was constructed, as shown in Fig. 3.1, with symmetrical coaxial input and output lines and tunable cavities which will allow an InSb photoconductive detector to be placed at one focus of a confocal elliptical radiation plate while the GaAs emitting structure is at the other focus.

It was considered advisable in the initial experiments, however, to use a detector which does not require cooling and whose use is well established. The logical choice is the Golay cell which has been used successfully to detect radiation from the ultraviolet out to the 50 Gc region. As shown schematically in Fig. 3.1, the Golay cell has a radiation absorbing membrane which has a mirror surface on its reverse side. A lens focuses an internal light beam onto this surface which reflects the beam to a photodetector. As radiation is absorbed, the membrane vibrates due to gas collision, thus modulating the internal light beam. One potential limitation of the Golay cell is its response time of 15 msec which is incompatible with the nanosecond pulses required by Gunn[6] to avoid overheating of his specimens. This can be overcome by the much improved heat sink arrangement which was designed for use in these experiments and by suitable modulation of a pulse train.

To establish the existence of submillimeter and far infrared radiation, a 0.120 in. x 0.120 in. cross-section waveguide, 0.600 in.

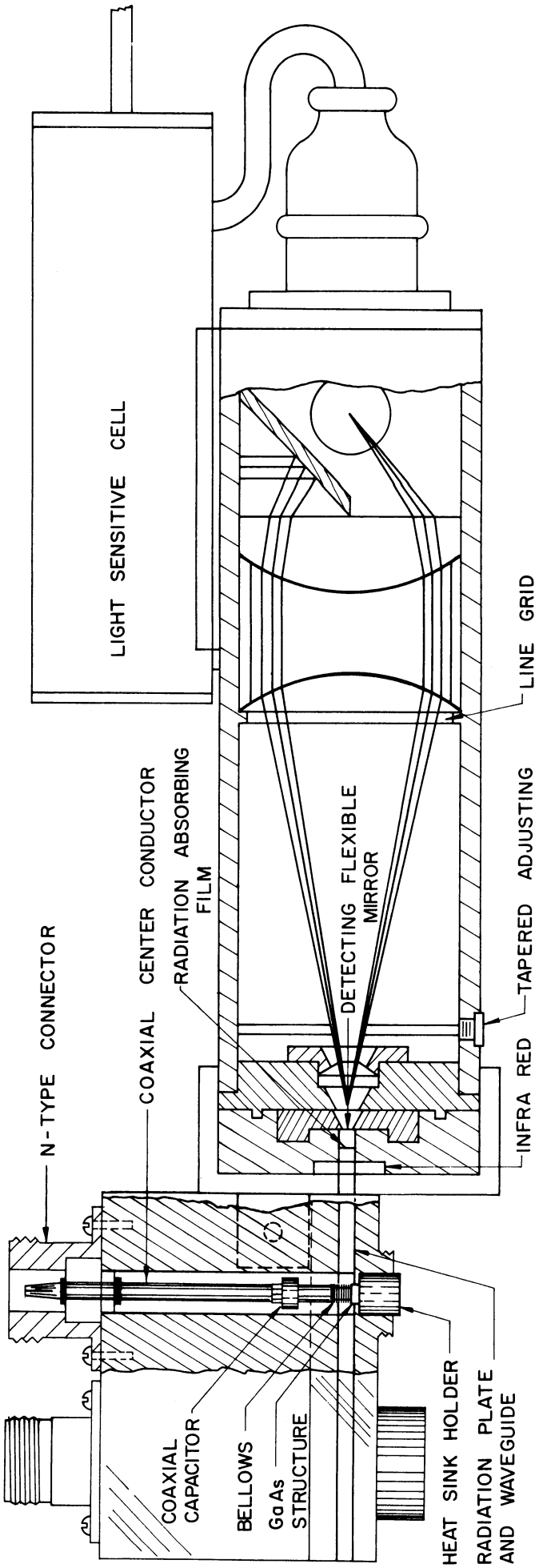

FIG. 3.1 COAXIAL SEMICONDUCTOR RADIATION MOUNT AND GOLAY CELL.

long, is coupled into the coaxial microwave cavity as shown in Fig. 3.1. Since this waveguide section is cut off below 50 Gc, radiation as high in frequency as 6 Gc will be reduced by at least 1000 db (about 27 db for every length a = 0.120 in. of the waveguide). This, along with the low frequency response limit of about 50 Gc for the Golay cell, insures that any observed radiation is at least above 50 Gc with no monochronometer between the source and Golay cell.

In the initial experiments to ascertain the existence of far infrared radiation, a two megohm impedance, four-stage transistorized preamplifier was designed with a flat response from about 15 cps to above 100 kc. This was followed by a low-pass filter network to peak the overall response of the preamplifier at 20 cps with a voltage gain of 100. This drastically reduced the noise output of the photodetector high-impedance transistor preamplifier circuits.

Two methods were devised to produce a radiation signal which could be detected with the 15 msec response time of the Golay cell. In the first method a low duty cycle pulse train is generated by triggering a HP-212A pulse generator from a transistorized free running multivibrator. This 100-1000 pps pulse train is square-wave modulated at 20 cps with a transistor holding one of the multivibrator stages in the "on" condition for half the period.

In the second approach, a mercury wetted relay circuit is used to switch up to 20 amps of current at a 10-20 cps rate, with a 50 percent duty cycle, directly into the GaAs structure. With a good heat sink arrangement, such long current pulses are possible without heating damage to the crystal.

With the latter 20 cps square-wave modulated current source, radiation was initially detected in the frequency range above 50 Gc

using the circuit shown in Fig. 3.2. The preamplifier output increased to 70 mv peak-to-peak with 20 amperes of current being switched into a 0.048 in. x 0.056 in. structure ($J = 1150$ amps/cm^2). However, since the Golay cell has a flat frequency response it is necessary to utilize a grating spectrometer to determine the radiation spectrum.

3.3.3 Radiation Frequency Spectrum. A Perkin-Elmer (Model 301) Far Infrared Double Beam Spectrometer was used to evaluate the frequency spectrum of the radiation. To utilize this instrument the internal globar and mercury H-4 sources were switched off and instead the GaAs source, in the mount shown in Fig. 3.1, was positioned where the specimen is normally located during absorption measurements. With an internal circuit change and external switching source it was possible to synchronize the 211-A square-wave generator to the internal 13 cps chopping rate of the spectrometer. The output was then maximized by positioning the beam emitted by the GaAs structure through the 0.6 inch long, 50 Gc cutoff waveguide. The exit of the radiation mount was placed approximately five inches from the entrance to the monochrometer in a chamber flushed with dry nitrogen gas to reduce the water vapor absorption lines.

This instrument is designed to operate in the region from 25 μ to 200 μ and has diffraction gratings available with lines spaced by 125.0 μ, 50.0 μ, 33.3 μ and 25.0 μ. These gratings are blazed for maximum reflection at 112.5 μ, 45.0 μ, 30.0 μ, and 22.5 μ, respectively.

Figure 3.3 shows a chart recorder plot of the emitted radiation as the angle of grating is varied from 22.5° to 27.5°, for three different conditions. The longest available integration response time (15.0 minutes/angular degree) was used to give good resolution. The radiation path

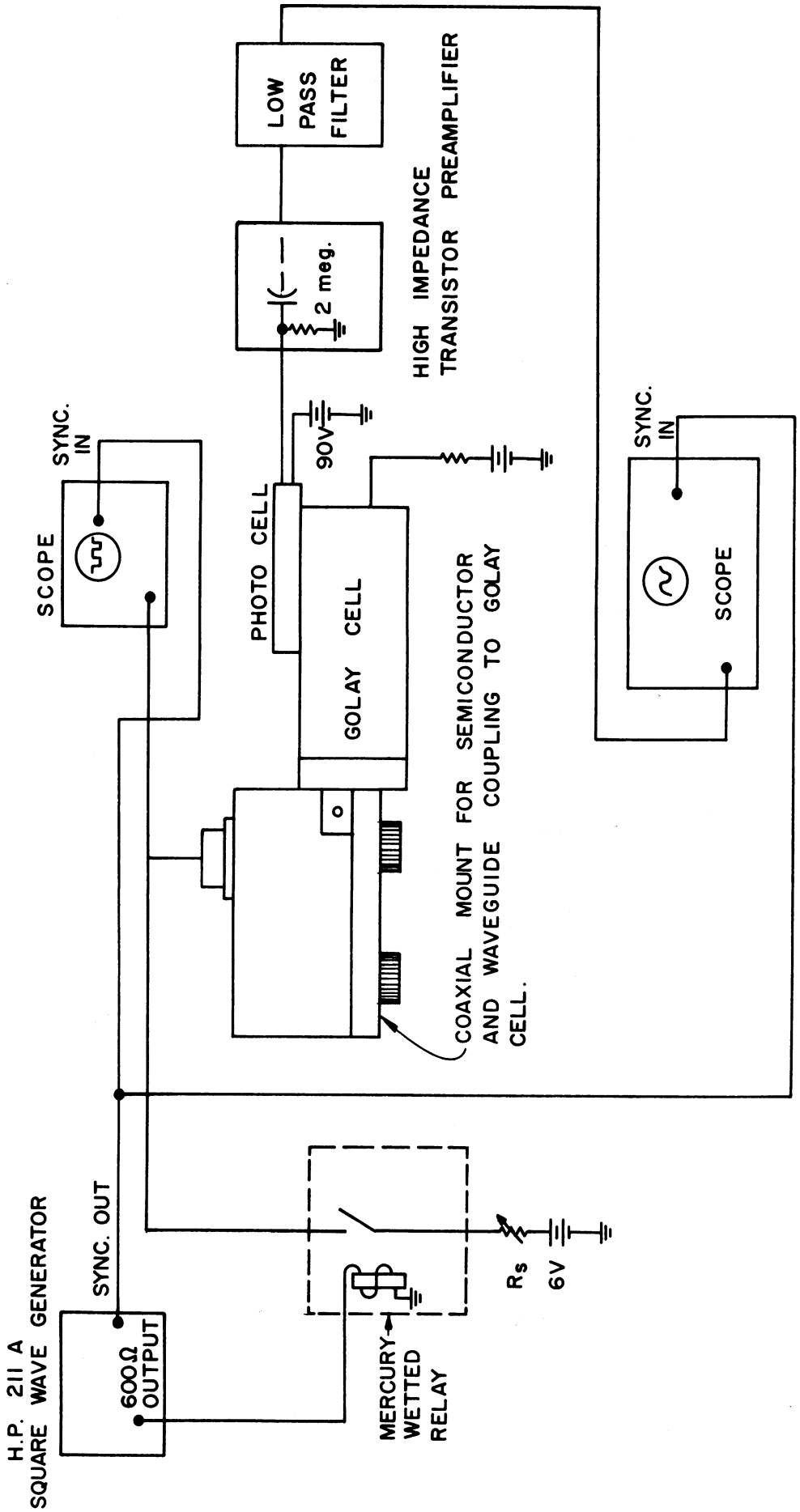

FIG. 3.2 INFRARED RADIATION DETECTION CIRCUIT FROM GaAs STRUCTURES.

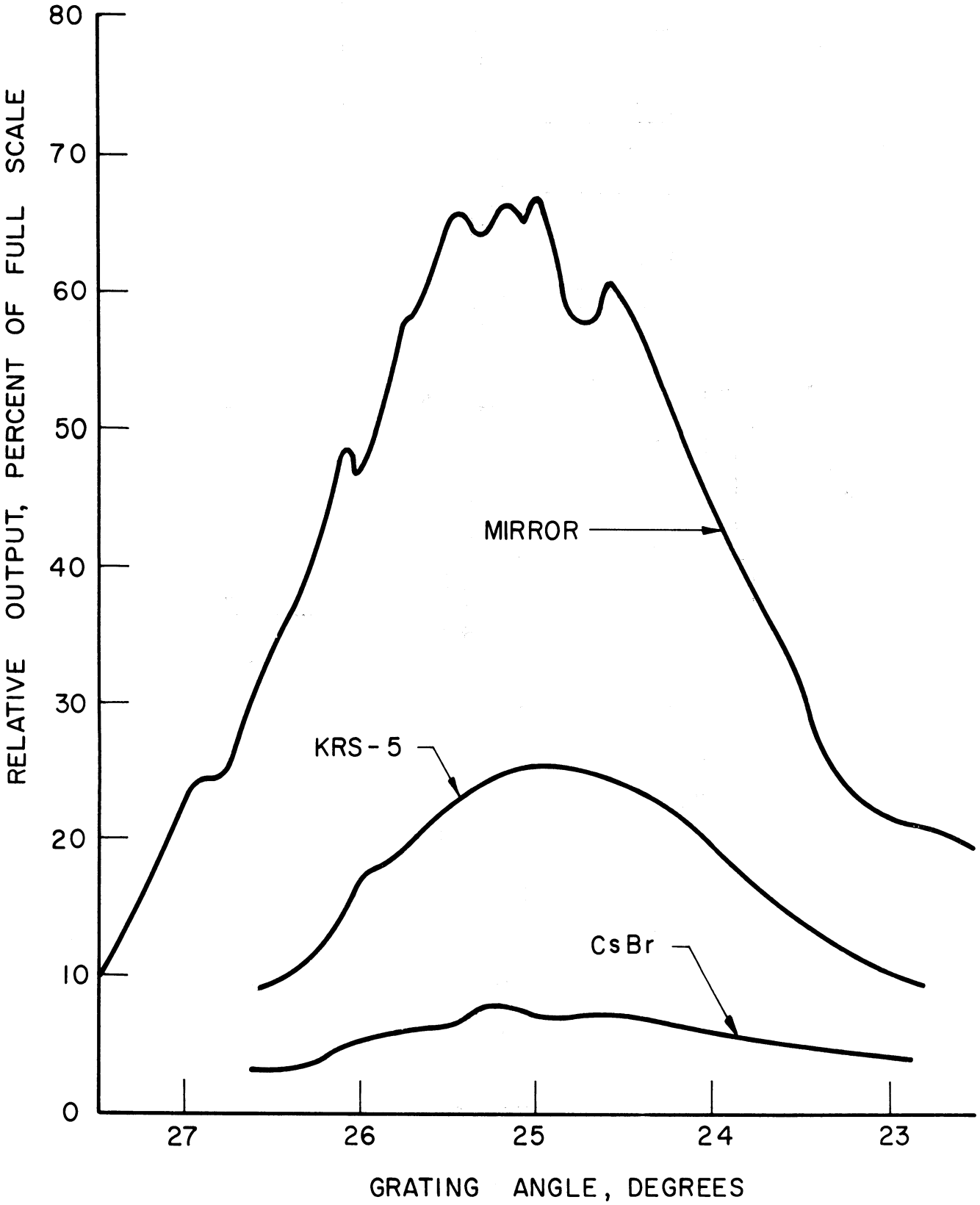

FIG. 3.3 SPECTRAL OUTPUT VS. ANGLE OF 125 μ GRATING FOR MIRROR OR RESTSTRAHLEN FILTERS. CURRENT DENSITY = 535 AMPS/CM^2.

consists of eight separate focusing mirrors, a continuously driven diffraction grating and a Golay cell detector.

In order to be positive that radiation lies in a certain spectral region it is necessary to ascertain whether higher-order effects are occurring at the grating and that Reststrahlen filters give the expected attenuation in the radiation spectrum based on their reflection curves. Analysis has revealed that the radiation spectrum shown in Fig. 3.3 is very probably due to radiation longer than the 25 μ - 200 μ region covered by this spectrometer. This conclusion has been reached because the 125 μ, 50 μ and 33.3 μ gratings give a spectral maximum at nearly the same grating angle. This would indicate that radiation from the GaAs source is of a longer wavelength and is causing specular reflection to occur from the blazed surface of the gratings. This was first indicated by the use of Reststrahlen filters of KRS-5 and CsBr. Reflection data[8] shows that the latter has a peak (90 percent) reflection curve centered at 122 μ while the former has a broad peak at 180 μ and remains above 60 percent reflection out beyond 400 μ.

If the energy spectrum shown in Fig. 3.3 for a mirror reflector occurred in the first order of the 125 μ grating this would indicate that the spectrum is centered at 104 μ. However, with a KRS-5 Reststrahlen filter replacing that particular mirror in the system, the middle curve resulted. The lower, nearly constant, curve resulted from the CsBr Reststrahlen filter. A similar nearly flat spectrum resulted from NaCl which has a 90 percent reflection peak at 53 μ and drops off rapidly at

---

8. Mitsuiski, A., Yamada, Y. and Yoshinaga, H., "Reflection Measurements on Reststrahlen Crystals in the Far-Infrared Region", Jour. of Opt. Soc. of Am., vol. 52, pp. 14-16; January, 1962.

longer wavelengths. The conclusion is that specular reflection must be occurring at the same grating blaze angle due to radiation longer than 200 μ and that a substantial amount of this radiation is being reflected by the KRS-5 to beyond 400 μ while the other Reststrahlen filters are absorbing the radiation in this longer wavelength region.

The exact shape of the radiation spectrum and its center frequency must thus be determined during the next reporting period. A spectrometer will be used which will incorporate coarser gratings for use out to 1000 μ. At least part of the band shape in Fig. 3.3 could be due to band characteristics of the variable angle specular reflection since the finely ruled grating is not operating in its normal fashion. Peaking in the spectral shape with increased current density is revealed in Fig. 3.4, however.

Figure 3.4 shows just the central portion of the same spectral region under the same conditions except that the 13 cps pulsed current density has been changed to evaluate the change in spectrum with current density. It can be seen from Fig. 3.4 that the radiated spectrum from the lowest current density (345 amp/cm^2) is very smooth; however, as the current density is increased, fine structure appears in the spectrum. For the highest current density (715 amps/cm^2) the spectrum becomes more peaked. To determine accurately the radiation threshold and rate of change of radiated power with current density, the spectrometer grating was set at the stationary center band position and the digital output was recorded with changes in current density.

Figure 3.5 shows the threshold condition with the maximum sensitivity of the Golay cell detector. Radiation is first detected at 50 amps/cm^2 and the output is linearly asymptotic to 90 amps/cm^2. At 435

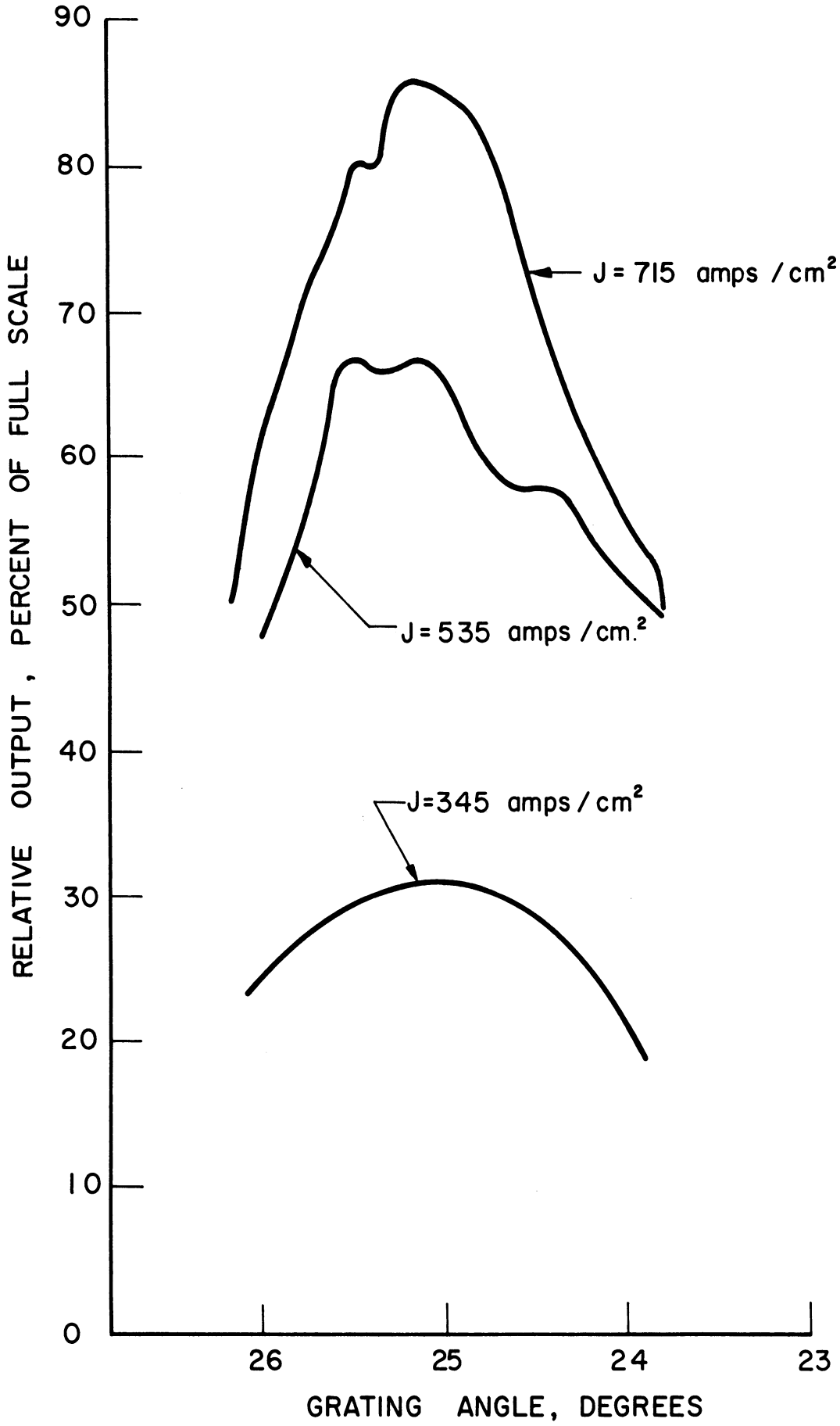

FIG. 3.4 SPECTRAL OUTPUT VS. ANGLE OF 125 μ GRATING FOR VARIOUS CURRENT DENSITIES.

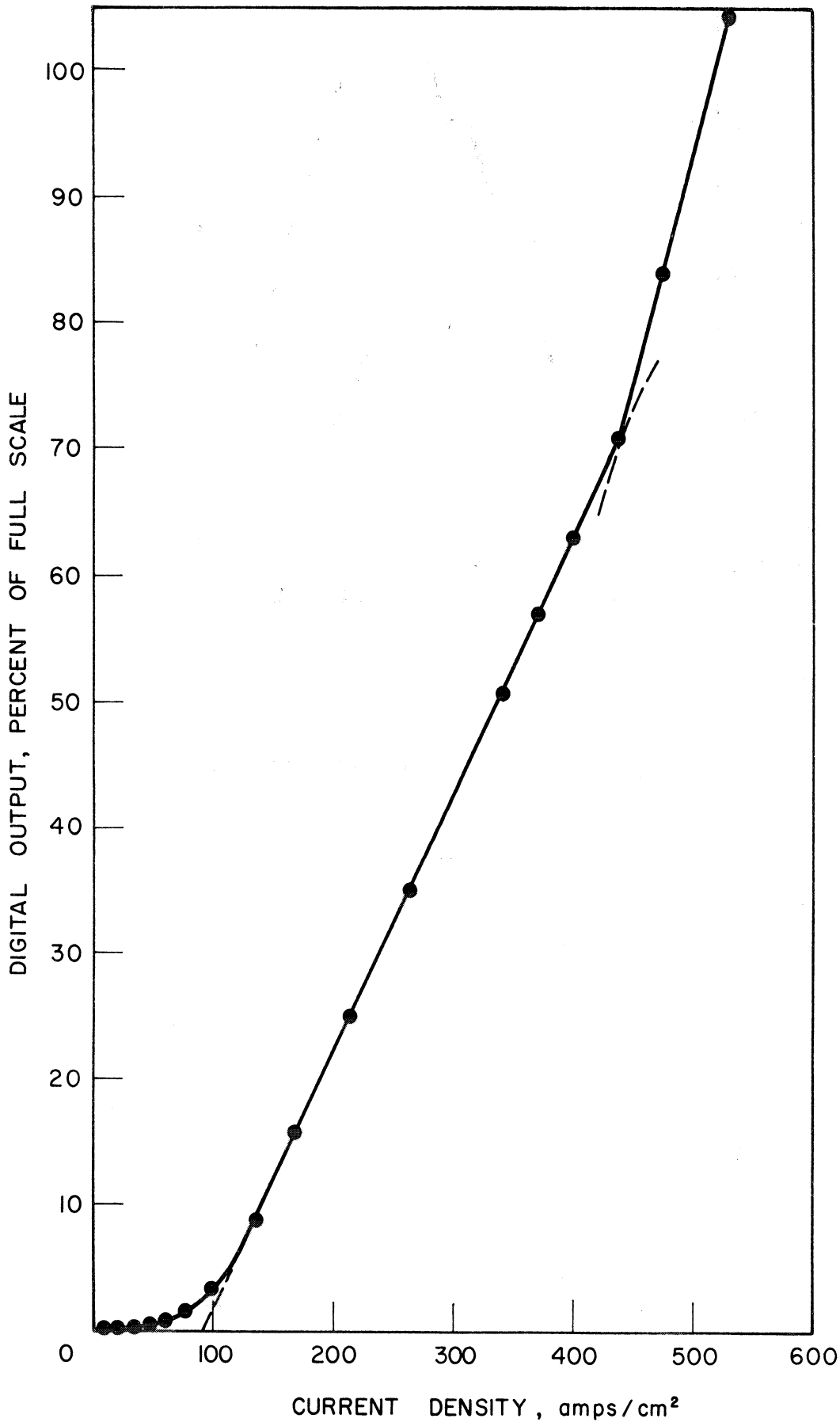

FIG. 3.5 SPECTRAL OUTPUT AT CENTER BAND AND THRESHOLD CONDITION VS. APPLIED CURRENT DENSITY.

amps/cm^2 there appears to be an abrupt transition to a higher slope region corresponding to the narrowing in the spectrum in Fig. 3.4.

It seems highly improbable that the observed radiation could be due to a black body heat source as can be seen from examining Planck's law and Wien's law. The latter shows that, considering a GaAs crystal at 500°K, the wavelength at maximum heat intensity is

$$\lambda_{max} = \frac{2897\ \mu - °K}{500°K} = 5.79\ \mu \quad .$$

Thus λ_{max} is considerably shorter than the wavelength of more than 200 μ indicated for the detected radiation.

In addition, assuming T = 500°K and crystal edge area = 5 x 10^{-3} cm^2, Planck's law shows that the emitted energy per μ drops from 1.1 x 10^{-4} watts/μ at λ = 10 μ to 5.6 x 10^{-8} watts/μ at λ = 100 μ. Thus, not only is the thermal power small at this temperature and crystal area but it also drops off very rapidly with increased wavelength in the region beyond 10 μ.

Wien's second law states that

$$W_{\lambda max} = 1.3\ T^5 \times 10^{-15}\ \frac{\text{watts}}{\text{cm}^2 \cdot \mu} \quad .$$

There is a strong T^5 temperature dependence of thermal radiation peak which is inconsistent with the linear output vs. current density plot shown in Fig. 3.5. The conclusion is that the n-ohmic-n GaAs source described in this report represents a source quite distinct from a thermal source in the region beyond 100 μ.

3.4 Conclusion. Substantial radiation has been detected in the region above 50 Gc with current densities greater than 50 amps/cm^2 in n-ohmic-n GaAs structures. Output is nearly linear with applied current

density. Data presented in this report strongly indicate that the radiation wavelength is longer than 200 μ. This is consistent with the the report by Gunn[6] that he has failed to find radiation from the visible out to 55 μ. No definite measure of the absolute power of this far infrared radiation is available at this time; however, in the Perkin-Elmer Model 301 spectrometer sensitivity is comparable to that with the internal globar and mercury H-4 sources which supply many watts of power.

It is believed that this is the first report of significant far infrared radiation from bulk electrical transport processes in III-V semiconductors.

3.5 Program for the Next Quarter. During the next quarter the GaAs radiation mount will be operated in a vacuum far infrared spectrometer suitable for the 200 - 1000 μ region because of coarser gratings. It is hoped that this will reveal the center frequency and spectrum of the radiation.

Structures will be ordered with different doping concentrations since it is felt that the donor ionization energy will play a significant role in the frequency selection process for stimulated emission of Bremsstrahlung radiation. Data[9] indicates that in n-type GaAs at an inpurity concentration of $8 \times 10^{16}/cm^3$ the impurity ionization energy is 0.003 ev, corresponding to a wavelength of 400 μ. Ohmic-p-ohmic GaAs structures will also be evaluated in the light of the discussion of this report.

Effort will be directed toward producing small area GaAs structures since this will allow study of a possible second threshold

---

9. Bloom, R. F., Barrie, R. and Ross, J. M., "Semiconductors and Phosphors", In Proceedings of International Colloquium at Garmissh-Partenkirchen, Friedr Vieweg and Sohn, p. 453; 1958.

for interaction of the internally generated, far infrared radiation with optical phonon vibrational modes to produce microwave radiation. Reports indicate that the current threshold for observed microwave radiation is an order of magnitude higher than the highest current density of 715 amps/cm^2 investigated in this report.

4. Traveling-Wave Phonon Interactions (J. E. Rowe, C. Yeh)

4.1 Longitudinal Acoustic-Wave Amplifier. Some of the material of Interim Scientific Report No. 1 must be modified as a result of correcting* the Poisson's equation. Poisson's equation and the r-f current density are now defined as

$$\frac{\partial D_1}{\partial z} = \rho_1 \tag{4.1}$$

and

$$J_1 = u_o\rho_1 + \rho_o u_1 - \mu \frac{kT}{q} \frac{\partial \rho_1}{\partial z} \quad . \tag{4.2}$$

The first term on the right-hand side of Eq. 4.2 can be identified as the convection current density, the second term as the conduction current density which is proportional to E, as $u_1 = \mu E_1$, where μ is the mobility of the carrier. The last term can be identified as the diffusion current density with $(\mu kT/q)$ as the diffusion constant. Following Hutson, McFee and White[1], it is convenient to define characteristic frequencies as

---

* This correction was also pointed out by Mr. J. Sizelove of the Electronic Technology Division.

1. Hutson, A. R., McFee, J. H. and White, D. L., "Ultrasonic Amplification in CdS", Phys. Rev. Letters, vol. 7, pp. 237-239; September 15, 1961.

$$\omega_c \triangleq \frac{\mu\rho_o}{\epsilon} \quad \text{(conductivity frequency)},$$

$$\omega_D \triangleq \frac{qu_o^2}{\mu kT} \quad \text{(diffusion frequency)} \quad . \tag{4.3}$$

Equation 4.2 is now rewritten as

$$J_1 = u_o\rho_1 + \epsilon\omega_c E_1 - \frac{u_o^2}{\omega_D}\frac{\partial\rho_1}{\partial z} \quad . \tag{4.4}$$

The continuity equation in a one-dimensional case is

$$\frac{\partial J_1}{\partial z} + \frac{\partial\rho_1}{\partial t} = 0 \quad . \tag{4.5}$$

Combining Eqs. 4.1, 4.4 and 4.5 yields

$$\frac{\partial^2 D_1}{\partial z\partial t} = -u_o\frac{\partial^2 D_1}{\partial z^2} - \epsilon\omega_c\frac{\partial E_1}{\partial z} + \frac{u_o^2}{\omega_D}\frac{\partial^3 D_1}{\partial z^3} \quad . \tag{4.6}$$

Applying the exponential operator and solving for D_1 yields the following result:

$$D_1 = \frac{j\epsilon(\omega_c/\omega)E_1}{1 - (u_o/v) - j(u_o/v)^2(\omega/\omega_D)} \quad . \tag{4.7}$$

Now with a knowledge of E_1 and D_1, T and S can be found from the equations of state as

$$T = c'S \quad , \tag{4.8}$$

where

$$c' = c\left[1 + \frac{e^2}{c\epsilon}\left\{\frac{1 - (u_o/v) - j(u_o/v)^2(\omega/\omega_D)}{1 - (u_o/v) - j(u_o/v)^2(\omega/\omega_D) - j(\omega_c/\omega)}\right\}\right] . \tag{4.9}$$

From c' an attenuation constant can be found:

$$\alpha = \frac{\omega}{v} c^{1/2} I_m (c'^{-1/2})$$

$$= \frac{\omega}{v_o} \frac{e^2}{2c\epsilon} \frac{\omega_c/\gamma\omega}{1 + (\omega_c/\gamma\omega)^2 [(1-\gamma)^2 (\omega^2/\omega_c\omega_D) + 1]^2} , \qquad (4.10)$$

where $\gamma = 1 - u_o/v$,

$v_o = \sqrt{c/\rho_m}$ = the unperturbed acoustic velocity.

The scale factor $e^2/c\epsilon$ is an electromechanical coupling constant which is proportional to the ratio of mechanical to electrical energy stored in the medium. It can be seen that if $u_o > v$, i.e., if the drift velocity of the carriers is maintained at a value slightly greater than the acoustic wave velocity in the medium, γ becomes negative and so is the attenuation constant α. In other words, acoustic gain instead of attenuation results.

If one introduces a modified Debye length defined as

$$\Lambda^2 \triangleq [\omega^2/\omega_c\omega_D k^2] (1 - \gamma)^2 \qquad (4.11)$$

into Eq. 4.10 the following results:

$$\alpha = \frac{\omega}{v_o} \frac{e^2}{2c\epsilon} \frac{\omega_c/\gamma\omega}{1 + (\omega_c/\gamma\omega)^2 (k^2\Lambda^2 + 1)^2} \qquad (4.12a)$$

or

$$[\alpha] \triangleq \frac{\alpha v_o}{\omega(e^2/2\, c\epsilon)} = \frac{\gamma\omega/\omega_c}{(\gamma\omega/\omega_c)^2 + (k^2\Lambda^2 + 1)^2} . \qquad (4.12b)$$

$[\alpha]$ is the normalized attenuation (or gain) constant. Since $\gamma\omega/\omega_c$ and $k^2\Lambda^2 + 1$ always appear as individual entities, they can be treated as variable and/or parameters respectively. Figure 4.1 is a plot of Eq.

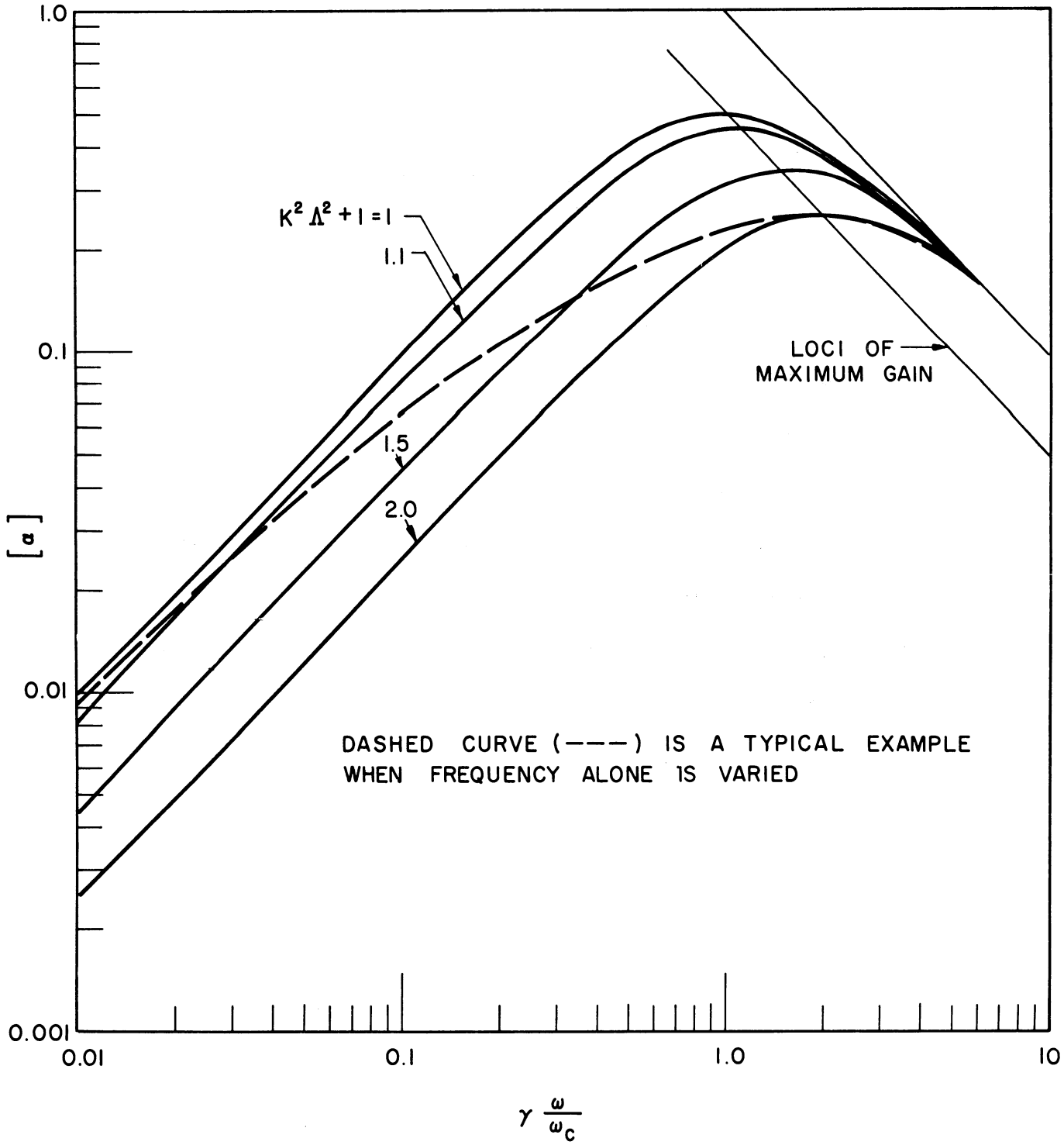

FIG. 4.1 NORMALIZED GAIN (OR ATTENUATION) $[\alpha]=(\alpha v_o/\omega)/(e^{<}/2c\epsilon)]$ VS. NORMALIZED FREQUENCY $\gamma\omega/\omega_c$ FOR VARIOUS VALUES OF THE PARAMETER $k^2\Lambda^2 + 1$.

4.12b using $\gamma\omega/\omega_c$ as a variable and $(k^2\Lambda^2 + 1)$ as a parameter. Notice that - $[\alpha]$ is plotted as positive for convenience. In using this plot to discuss the variation of the attenuator (or gain) constant with frequency, (consider $k^2\Lambda^2$ as a constant for the time being) it must be remembered that $[\alpha] \alpha 1/\omega$. At low frequencies where $(\gamma\omega/\omega_c) \ll (k^2\Lambda^2 + 1)$, α is actually proportional to ω^2. This situation is represented as a straight line with unity positive slope on the log-log plot of $[\alpha]$ vs. $\gamma\omega/\omega_c$. On the other hand, a straight line with a negative unity slope actually signifies frequency independence of α. This can be seen from Eq. 4.12b by letting

$$(\gamma\omega/\omega_c) \gg (k^2\Lambda^2 + 1)$$

so that

$$[\alpha] = \frac{\alpha v_o}{\omega(e^2/2\, c\epsilon)} = \omega_c/\gamma\omega \qquad (4.13)$$

or

$$\alpha = \frac{\omega_c}{\gamma v_o} \quad \frac{e^2}{2c\epsilon} = \text{constant} \quad .$$

Curves of the normalized $[\alpha]$ for various values of the parameter $(k^2\Lambda^2 + 1)$ show a general pattern of increase with increasing $\gamma\omega/\omega_c$ at lower values of $\gamma\omega/\omega_c$ and then gradually leveling off toward a maximum indicated by

$$[\alpha]_m = \frac{1}{2(k^2\Lambda^2 + 1)} \qquad (4.14)$$

which occurs at $(\gamma\omega/\omega_c) = k^2\Lambda^2 + 1$. From there on, the curves fall off asymptotically toward a straight line given by Eq. 4.13. Notice that the loci of the maximum $[\alpha]$ also follows a line parallel to this

straight line. This indicates that the maximum attenuation (or gain) constant is also frequency independent.

The above discussion is strictly true only when $k^2\Lambda^2$ = constant. According to Eq. 4.11, $k^2\Lambda^2 = (1-\gamma)^2\omega^2/\omega_c\omega_D$, indicating that for a constant drift velocity u_o and a near constant acoustic velocity v, $k^2\Lambda^2$ is proportional to ω^2. Thus, at lower frequencies, when $k^2\Lambda^2$ is small, the gain curve [α], calculated for say, $k^2\Lambda^2 = 1$ (or $k^2\Lambda^2 + 1 = 2$), is actually too conservative. In other words, the actual [α] curve would run from the curve marked $k^2\Lambda^2 + 1 = 1$, crossing all curves of $1 \leq (k^2\Lambda^2 + 1) \leq 2$ to reach the point of maximum gain on the $k^2\Lambda^2 + 1 = 2$ curve and then cutting back into the curves for $k^2\Lambda^2 + 1 > 2$. A typical curve of this kind is shown as the dotted line in Fig. 4.1.

The significance of the parameter $k^2\Lambda^2 + 1$ needs further explanation. From Eq. 4.11, it is clear that $k^2\Lambda^2$ is intimately related to the conductivity and diffusion frequencies. Since $\gamma = 1 - u_o/v$ is usually a small negative number for practical amplifiers, then $1 - \gamma \simeq 1$ and $k^2\Lambda^2 \simeq \omega^2/\omega_c\,\omega_D$. Thus $k^2\Lambda^2 + 1 = 2$ (or $k^2\Lambda^2 = 1$) would actually specify $\omega^2 = \omega_c\omega_D$, or $(\omega_c/\omega) = (\omega/\omega_D)$. In other words, the conduction current equals the diffusion current. This is also the condition for maximum gain if ω alone is varied.

$k^2\Lambda^2 = 0$ (or $k^2\Lambda^2 + 1 = 1$) is a limiting case at low frequencies. At these frequencies, $(\omega_c/\omega) \gg (\omega/\omega_D)$. In other words, the ratio of conduction to diffusion current is much greater than unity. The maximum gain becomes

$$\alpha_m = \frac{\omega_c}{v_o}\,\frac{e^2}{2c\epsilon}\,\frac{1}{2\gamma} \quad . \tag{4.15}$$

Now let $N = (\omega/2\pi v_o)\, L = L/\lambda$ = the length of the crystal in acoustic wavelengths, then the maximum gain in db is given by

$$G_{max} = 27.3 \left(\frac{e^2}{2c\epsilon} \right) N \text{ db} \quad . \tag{4.16}$$

For $k^2\Lambda^2 + 1 > 2$, or $k^2\Lambda^2 > 1$, or $\omega/\omega_c > \omega_D/\omega$ one has a high frequency case and the gain is reduced accordingly.

Equation 4.9 can also be used to derive the equation for the acoustic velocity. It can be shown that the acoustic velocity of propagation is given by

$$v = \frac{\text{Real}\sqrt{c'}}{\sqrt{\rho_m}} = v_o \frac{\text{Real}\sqrt{c'}}{\sqrt{c}} \quad . \tag{4.17}$$

Use of Eq. 4.9 and carrying out the indicated manipulations in Eq. 4.17 yields

$$v = v_o \left\{ 1 + \frac{e^2}{2c\epsilon} \frac{1 + (\omega_c/\gamma\omega)^2 k^2\Lambda^2 (k^2\Lambda^2 + 1)}{1 + (\omega_c/\gamma\omega)^2 [k^2\Lambda^2 + 1]^2} \right\} \tag{4.18a}$$

or

$$[v] = \frac{v - v_o}{e^2/2c\epsilon} = \frac{(\gamma\omega/\omega_c)^2 + k^2\Lambda^2 (k^2\Lambda^2 + 1)}{(\gamma\omega/\omega_c)^2 + (k^2\Lambda^2 + 1)^2} \quad , \tag{4.18b}$$

where v_o is the unperturbed acoustic velocity $= \sqrt{c/\rho_m}$. A plot of $[v]$ vs. $\gamma\omega/\omega_c$ with $k^2\Lambda^2 + 1$ as parameters results in a universal graph as shown in Fig. 4.2. Curves for constant $k^2\Lambda^2 + 1$ remain horizontal at smaller values of $\gamma\omega/\omega_c$ at their respective zero frequency limiting values corresponding to $k^2\Lambda^2/(k^2\Lambda^2 + 1)$ and increase asymptotically to unity, the upper limit at infinite frequency.

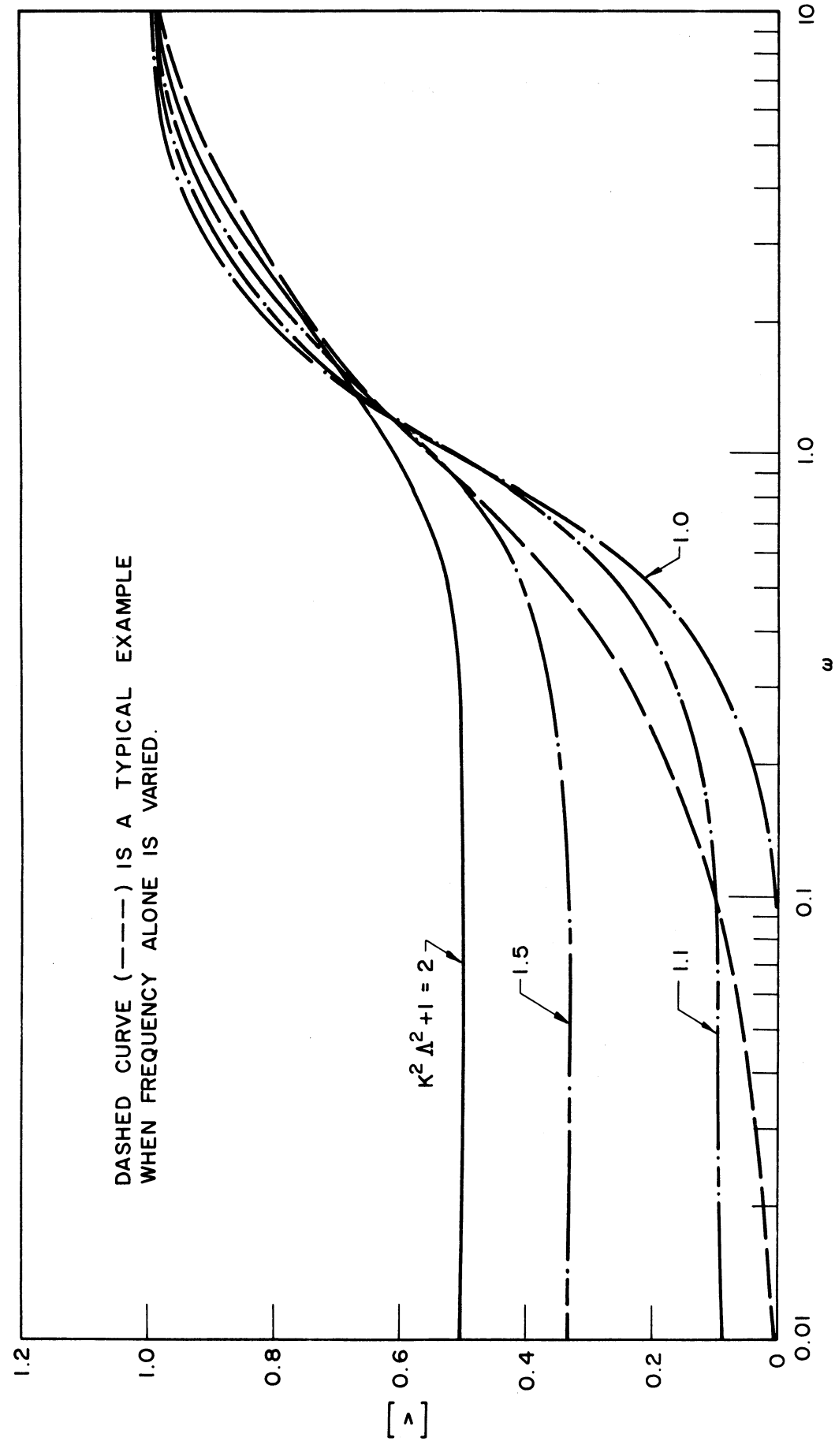

FIG. 4.2 NORMALIZED ACOUSTIC VELOCITY [v] [= $\{(v-v_o)/v_o\}/(e^2/2c\epsilon)$] VS. FREQUENCY $\gamma\omega/\omega_c$ FOR VARIOUS VALUES OF THE PARAMETER $k^2\Lambda^2 + 1$.

If Fig. 4.2 is used to discuss the variation of [v] with frequency, it must be remembered that the parameter $k^2\Lambda^2 + 1$ also varies with frequency. The dotted curve indicates one typical variation of [v] with frequency.

4.2 ω-k Diagram for a Longitudinal Acoustic-Wave Amplifier. The equation for calculating the acoustic velocity in a phonon-wave amplifier has been derived in a previous report and is rewritten here as

$$\frac{v - v_o}{v_o e^2/2c\epsilon} = \frac{\left(1 - \frac{u_o}{v}\right)^2 + \frac{\omega}{\omega_d}\left(\frac{\omega_c}{\omega} + \frac{\omega}{\omega_d}\right)}{\left(1 - \frac{u_o}{v}\right)^2 + \left(\frac{\omega_c}{\omega} + \frac{\omega}{\omega_d}\right)^2} \quad . \tag{4.19}$$

Notice that in deriving this equation, a diffusion frequency ω_d has been redefined in terms of ω_D, the original diffusion frequency such that $\omega_d = \omega_D(v/u_o)^2$. This is necessary in order to rid ω_D of a dependence upon the drift velocity u_o. It was pointed out previously that the interpretation of the expression in terms of the actual parameters of the amplifier is difficult due to the complexity of the interrelations. However, one useful form for interpretation is to find the ω-k diagram for the amplifier. Solving Eq. 4.19 and noticing that $v = \omega/k$, a fifth-order equation for ω is obtained. The result is

$$\omega^5 - v_o k(1 + A)\omega^4 + \left(1 + 2\frac{\omega_c}{\omega_d}\right)\omega_d^2\omega^3 - \omega_d^2 k\left[\, 2u_o + v_o \right.$$

$$\left. \cdot\left(1 + A + (2 + A)\frac{\omega_c}{\omega_d}\right)\right]\omega^2 + \omega_d^2\left[\, \omega_c^2 + 2u_o k^2 v_o(1 + A) + u_o^2 k^2 \,\right]\omega$$

$$- \omega_d^2 v_o k\left[\, \omega_c^2 + u_o^2(1 + A)k^2 \,\right] = 0 \quad , \tag{4.20}$$

where $A = e^2/2c\epsilon$.

To solve this equation numerically, k is assumed to be a real value, positive or negative. For a typical set of parameters, the roots of ω are easily found on a computer. Negative real roots of ω are rejected because they are physically unrealizable. Complex roots are retained as they help to identify the time instability of the amplifier. The results of the computation for a typical set of parameters are summarized and plotted in Fig. 4.3. There are five roots for ω. ω_1, which is the only positive real root of the system, varies linearly with k. This is perhaps the working mode of the amplifiers in which the phase and group velocities are the same. This makes the matching of the drift velocity of the electrons to the acoustic wave velocity a simple matter. There are two pairs of complex conjugate roots of ω, labeled as ω_2, ...ω_4, each with a prefix R_e or I_m to indicate respectively the real or imaginary part of the complex frequency. The real parts of these frequencies are very close to the positive real frequency ω_1 as is indicated by the dotted line beside ω_1. The imaginary parts of one pair of conjugate roots remain practically unchanged at 10^{10} cps while the other pair, which is much smaller in magnitude, remains virtually unchanged at lower values of k but increases with k for k values greater than 1000. The existence of these complex roots may indicate the possibility of time instabilities. However, whether oscillation will take place depends upon the boundary conditions appropriate to the crystal. Complex roots also exist for negative values of k and thus it is possible to have a backward-wave mode of oscillation.

Another approach to finding numerical solutions of Eq. 4.19 is to assume ω as positive and real and find the roots of k. In this way, a negative real root of k indicates a backward mode of propagation and a

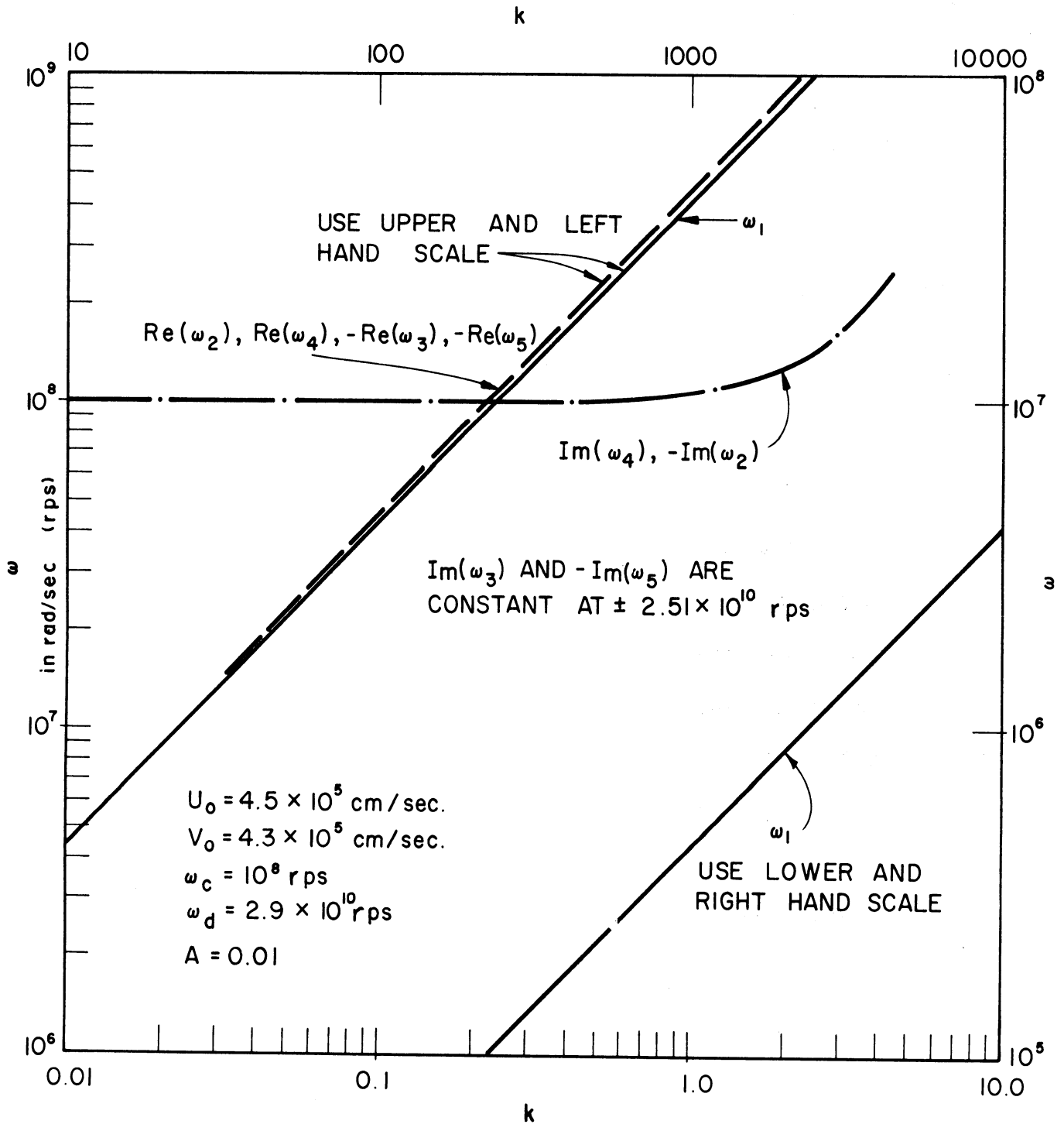

FIG. 4.3 ω-k PLOT OF A TYPICAL SET OF CRYSTAL PARAMETERS ASSUMING REAL VALUES OF k.

complex k may mean a space instability. For this purpose, Eq. 4.19 is rewritten in terms of descending powers of k. The result is

$$u_o^2 v_o (1 + A)k^3 - 2u_o \left[v_o (1 + A) + u_o/2 \right] \omega k^2$$

$$+ \left[2u_o + v_o (1 + A) + v_o \left(\frac{\omega_c}{\omega} + \frac{\omega}{\omega_d} \right) \left(\frac{\omega_c}{\omega} + \frac{\omega}{\omega_d} (1 + A) \right) \right] \omega^2 k$$

$$- \left[1 + \left(\frac{\omega_c}{\omega} + \frac{\omega}{\omega_d} \right)^2 \right] \omega^3 = 0 \quad . \qquad (4.21)$$

There are three roots of k, one real positive and a pair of complex conjugate roots. There is no negative real root of k, indicating that backward-wave modes are not likely. The imaginary part of the complex k is virtually constant for all values of ω up to 10^9 cps. The real part of the complex k follows close to but is slightly smaller than the real root of k. However, if ω_c is changed by a factor of 10 (smaller), the imaginary part of the complex k is reduced by almost tenfold and increases with increasing frequency. These results are plotted in Fig. 4.4.

4.3 Shear Mode Interactions. In the above sections the longitudinal wave interaction has been discussed in the derivation of the characteristic equation for phonon-wave amplifiers. It is interesting to investigate the characteristics for shear wave operation. Let us still limit our discussion to a one-mode solution. In a shear mode of operation, the conduction electrons produced by the drift field are moving in a direction perpendicular to the direction of propagation of the acoustic wave. Amplification of an acoustic wave can only take place if there is a mechanism which couples the shear waves to the drift current. Such a

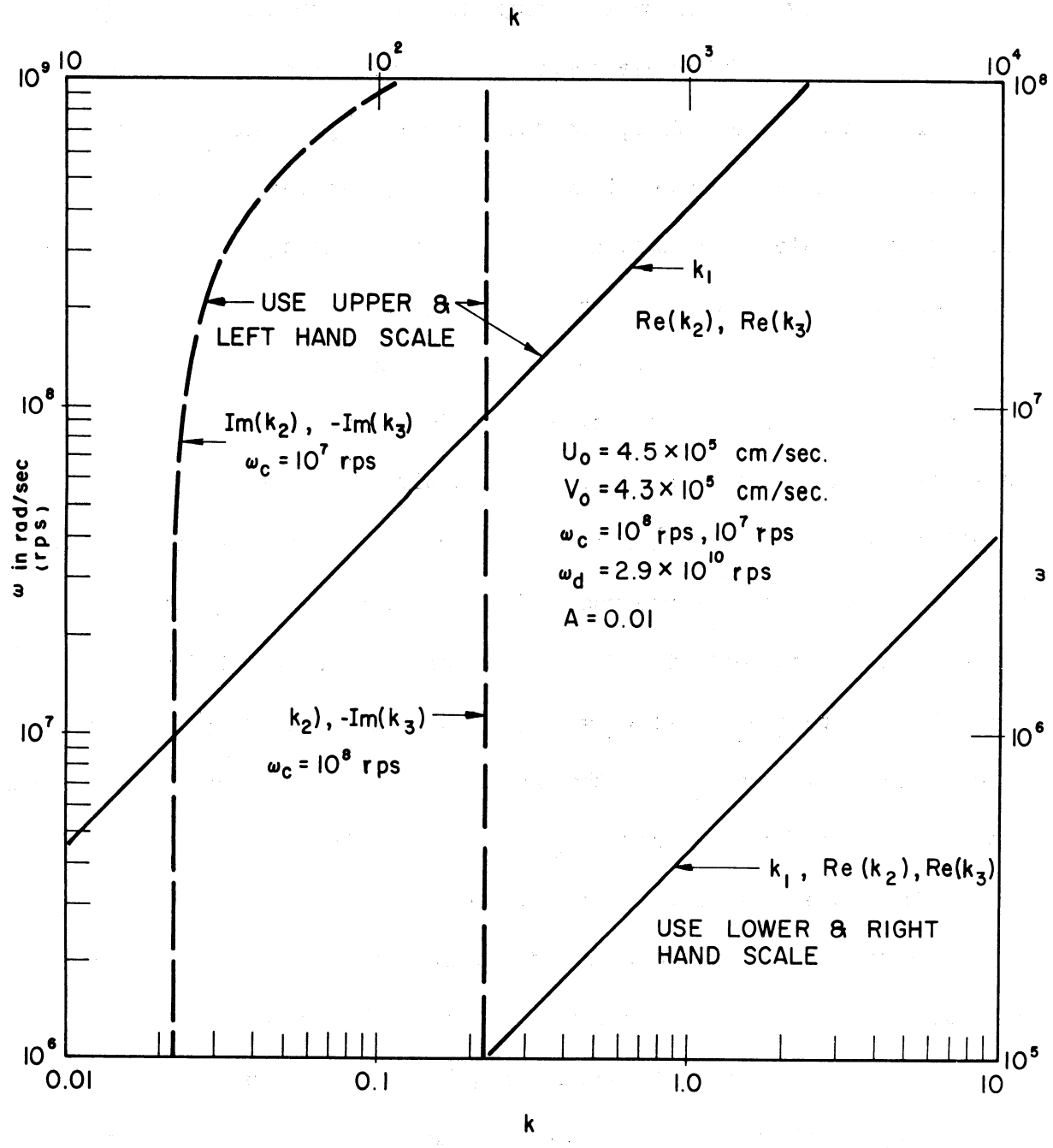

FIG. 4.4 ω-k PLOT FOR A TYPICAL SET OF CRYSTAL PARAMETERS, ASSUMING REAL POSITIVE ω.

mechanism is provided for by the longitudinal electric field (in the direction of the drifting electrons) of piezoelectric origin accompanying a transverse wave. Thus, one still needs only to solve a one-dimensional problem provided that the proper piezoelectric coefficient and elastic constant are chosen. Return now to the equations of state. These equations, in the most general form, result in tensors for the piezoelectric constants, the elastic constants and the dielectric constants. However, by assuming a one-mode solution and for a crystal of hexagonal symmetry, one can still use the simplified version of these equations for either longitudinal or shear wave modes provided that the appropriate coefficients are used. The effect of changing the mode of operation will manifest itself in two ways: the unperturbed acoustic velocity will be changed as $v_o = \sqrt{c/\rho_m}$, where c is actually c_{11} for the longitudinal wave and c_{44} for the transverse wave, also the piezoelectric constants e will be different, e_{333} in the e_{113} in the transverse mode.

The above statement was also made by Hutson and White[2], and Blötekjar and Quate[3] in their recent publications. Spector[4], using an entirely different approach, also verified this result. Spector's result is particularly worth mentioning, because it is quite general in nature. Spector's equation for the attenuation constant of a transverse

---

2. Hutson, A. R., White, D. L., "Elastic Wave Propagation in Piezoelectric Semiconductors", Jour. Appl. Phys.,vol. 33, No. 1, pp. 40-47; January, 1962.

3. Blötekjar, K. and Quate, C. F., "The Coupled Modes of Acoustic Waves and Drifting Carriers in Piezoelectric Crystals", Proc. IEEE, vol. 52, No. 4; April, 1964.

4. Spector, H. N., "Amplification of Acoustic Waves Through Interaction With Conductron Electrons", Phys. Rev., vol. 127, No. 4, pp. 1084-1090; August 15, 1962.

mode acoustic-wave amplifier which uses a piezoelectric crystal for the low frequency range is with proper correction*,

$$\alpha = \frac{1}{12\,\pi\rho v_s} \frac{q^2 t(1-\mu)\,(\omega/\omega_p)^2\, d_{xz}^{\,2}}{(1-\mu)^2(\omega/\omega_p)^4 + (\omega t)^2[1 + (1/3)\,(v_F/v_s)^2\,(\omega/\omega_p)^2]^2}\,, \tag{4.22}$$

where ρ is the mass density of the crystal,

v_s is the acoustic velocity,

q is the wave number,

t is the relaxation time,

$\mu = v_d/v_s$ is the ratio of drift velocity v_d to acoustic velocity v_s,

ω_p is the plasma frequency of the electrons,

v_F is the Fermi-velocity,

d_{xz} is the piezoelectric constant in the z-direction (longitudinal) due to transverse wave in the x-direction.

A careful study of his equation and ours reveals the following equivalences:

Spector's Notation	Our Corresponding Notation	Equivalence
ρ	ρ_m	$\rho = \rho_m$
v_s	v	$v_s = v$
q	k	$q = k$
v_d	u_o	$v_d = u_o$
$\mu = v_d/v_s$	γ	$u = 1-\gamma$

---

* The original equation has the term $12\,\pi\rho v_s$ multiplying the first term of the denominator which is obviously incorrect.

Spector's Notation	Our Corresponding Notation	Equivalence
ω_p^2	ω_c	$\omega_p^2 = (q/m\mu)\,\omega_c$
v_F	ω_d	$v_F^2 = 3u_o^2 q/\omega_d m\mu$
d	e	$d = e/\epsilon_o$
t	μ	$t = \mu m/q$

Substituting these equivalences into Eq. 4.22 and making the appropriate change of units from cgs to MKS practical units, it can be reduced to our equation for α provided v_s is approximated by $v_o = (c/\rho_m)^{1/2}$. Thus it can be concluded that the equation for the gain (or attenuation) constant is the same for the longitudinal or transverse wave mode provided the proper constants are used.

4.4 Gain Equation for the Phonon-Wave Amplifier-Transverse Wave Mode. Spector's[4] approach is based upon the degenerate statistics of the carriers and the Boltzmann transport equation. This is different from the approach adopted by White[5], as well as the work covered by this research. In the later work, it is assumed that the carriers obey a nondegenerate statistic and diffusion and continuity equations are used. Spector's approach seems to be more general than the other approach on two accounts: First, for the coupling mechanism between the phonon-wave and drifting electrons, he assumes the presence of a deformation potential. His theory can easily be extended to cover the other coupling mechanism, i.e., the piezoelectric coupling mechanism, by simply adding a new term to that effect. Second, his treatment is applicable to higher frequencies at which the acoustic wavelength in the crystal is comparable or even shorter than the mean free path of the carriers. Unfortunately, both

---

5. White, D. L., "Amplification of Ultrasonic Waves in Piezoelectric Semiconductors", Jour. Appl. Phys., vol. 33, pp. 2547-2554; August, 1962.

White's and our present theories are subject to these limitations, being a low frequency approach and limited to piezoelectric coupling only. It is therefore of great interest to study Spector s results and to convert them to a form usable in our present research.

For materials with large piezoelectric constants compared to the deformation potential the piezoelectric effect can be used to advantage in phonon-wave amplifiers. For example, the piezoelectric constant of CdS at frequencies up to 10^{13} cps is several orders of magnitude larger than its corresponding deformation potential. Spector carried out the derivation of this case for a transverse wave mode. These equations are presented below in converted form for piezoelectric effect devices.

For low frequencies such that $\lambda > \ell$, i.e., for the acoustic wavelength greater than the mean free path of the carrier, [or $q\ell < 1$]*, and for the condition that the piezoelectric effect is greater than the deformation potential and that $(\omega/\omega_c)(e_{xz}/\epsilon_o E) > 1$, [or $ed_{xz} > qC_{xz}$, $(\omega/\omega_p^2)(ed_{xz}/mv_s) > 1$], Spector's equation for α is just that derived by Hutson, et al.[1]. However, for high frequencies, $\lambda < \ell$, [or $q\ell > 1$, $(\omega/\omega_p^2)(ed_{xz}/mv_s) > 1$],

$$[\alpha] = \frac{\gamma(1-\gamma)^2 \dfrac{\omega^2}{\omega_c \omega_D}}{\left[1 + (1-\gamma)^2 \dfrac{\omega^2}{\omega_c \omega_D}\right]^2} , \qquad (4.23)$$

where $[\alpha]$ is the normalized gain (or attenuation) factor defined previously. Of course the piezoelectric constant and the elastic constants used for the normalization are those corresponding to the transverse

---

* Notations in the square brackets are those used by Spector.

wave mode. Equation 4.23 differs from Spector s original equation by a factor γ. If straightforward conversion were made, the numerator of Eq. 4.23 would contain a term γ^2. It is believed that the original equation has a misprint. Since $\gamma = 1 - u_o/v$, $[\alpha]$ becomes negative (amplification) only when $u_o > v$. Having a γ^2 term as a multiplier in the numerator destroys this property and $[\alpha]$ will always be positive, i.e., amplification is impossible. Using $\omega_d \triangleq (v/u_o)^2\omega_D$ as previously, Eq. 4.23 can be rewritten as

$$[\alpha] = \frac{\frac{\gamma\omega^2}{\omega_c\,\omega_d}}{\left[1 + \frac{\omega^2}{\omega_c\,\omega_d}\right]^2} . \qquad (4.24)$$

$[\alpha]$ has a maximum at $\omega^2 = \omega_c\,\omega_d$. It decreases very rapidly toward both the high and low frequency ends, at frequencies for which $\omega^2/\omega_c\omega_d > 1$, $[\alpha] \propto \omega_c\omega_d/\omega^2$, in other words, the gain is inversely proportional to the square of the frequency at a fixed product of $\omega_c\,\omega_d$. This is in disagreement with the prediction from our previous equation and represents a more realistic one as indicated by most experimental results. This is to be expected since our previous equation is not expected to be valid at frequencies such that $\lambda < \ell$.

4.5 Gain Equation for the Phonon-Wave Amplifier Using the Deformation Potential as a Coupling Mechanism. As phonon waves propagate within the crystal, the momentary change in compression (in a longitudinal wave) produces local variations in the size and shape of the unit cell. The changes in lattice constant will thus change the energy-band structure in the crystal. The change in energy-band boundaries may be seen to be substantially equivalent to the introduction

of a varying potential for an electron which is referred to here as the deformation potential. This effect is in general quite small in most crystals. Particularly for piezoelectric materials, the effect of deformation potential may be negligible in comparison with the corresponding piezoelectric effect. However, certain semiconductors which may be chosen for the phonon-wave amplifier due to their high carrier mobility may not have the desired piezoelectric effect, while the effect due to the deformation potential may be significant. A typical material of this kind is very pure n-type InSb. It has a mobility of 5×10^5 cm^2/volt-sec and the deformation potential constant C is about 10 ev.

Spector's equations for $[\alpha]$ for the longitudinal and transverse waves using deformation potentials are rewritten in terms of our present notation as follows (the details of conversion are omitted):

1. For the longitudinal wave (Equation 3.5b in Spector's paper) for $\lambda > \ell$, $\frac{\omega}{\omega_c} \frac{kC}{qE} > 1$

$$\alpha = \frac{N_o qE}{3c_z} \frac{\gamma \left(\frac{\omega}{\omega_c} \right)^2 \frac{k^2 C_{zz}^2}{q^2 E^2}}{\left(\gamma \frac{\omega}{\omega_c} \right)^2 + \left[1 + \frac{\omega^2}{\omega_c \omega_D} (1-\gamma)^2 \right]^2} , \qquad (4.25)$$

where C_{zz} is the deformation potential constant in the z-direction and c_{zz} is the elastic constant in the same direction. E is the drift field in the same direction.

For $\lambda < \ell$,

$$\alpha = \frac{\pi N_o qE}{2c_{zz}} \frac{\gamma(1-\gamma)^2 \frac{\omega}{\omega_D}\left[1 + \frac{\omega}{\omega_c}\frac{kC_{zz}}{qE}\right]^2}{\left[1 + \frac{\omega^2}{\omega_c\omega_D}(1-\gamma)^2\right]^2} \quad . \tag{4.26}$$

2. For the transverse wave for $\lambda > \ell$, $\frac{\omega}{\omega_c}\frac{k\,C_{xz}}{qE} > 1$

$$\alpha = \frac{N_o qE}{c_{xz}} \frac{k^2 C_{xz}^2}{q^2 E^2} \frac{\gamma\left(\frac{\omega}{\omega_c}\right)^2}{\left(\gamma\frac{\omega}{\omega_c}\right)^2 + \left[1 + \frac{\omega^2}{\omega_c\,\omega_D}(1-\gamma)^2\right]^2} \quad . \tag{4.27}$$

For $\ell > \lambda$, $\frac{\omega}{\omega_c}\frac{k\,C_{xz}}{qE} > 1$

$$\alpha = \frac{\pi N_o qE}{2c_{xz}} \frac{k^2 C_{xz}^2}{q^2 E^2} \frac{\gamma(1-\gamma)^2 \frac{\omega}{\omega_D}\left(\frac{\omega}{\omega_c}\right)^2}{\left[1 + \frac{\omega^2}{\omega_c\omega_D}(1-\gamma)^2\right]^2} \quad . \tag{4.28}$$

The physical significance of these equations will be discussed in the next report.

4.6 Phonon-Wave Amplifier Transducers. One of the principle limitations to acoustic-wave amplifier performance is the very high coupling loss associated with the usual $\lambda/2$ x-cut quartz transducers which are in general glued to the piezoelectric material. In addition to high coupling loss such transducers are generally limited to the frequency region below 1 Gc.

During the past month a CdS rod has been equipped with thin film diffused copper layer transducers and is mounted in a coaxial line structure. Such a transducer should operate at high frequencies although no specific experimental data is yet available. Measurements

below 100 mc indicate strong echoes and suggest good coupling efficiency compared to the quartz transducers.

A more promising approach appears to be the utilization of thin insulating CdS films as transducers. The films are to be deposited by vacuum evaporation and the thickness for fundamental resonance is $t = \lambda/2$. The necessary film thickness is shown vs. frequency in Table 4.1 assuming that the compressional velocity along the c-axis of CdS is 4.4×10^5 cm/sec.

Table 4.1

CdS Film Thickness Vs. Frequency

$v = 4.4 \times 10^5$ cm/sec

f(Gc)	Thickness $t = \lambda/2$
1	2.2 microns
3	0.72 microns
10	0.22 microns
30	720 Å
50	440 Å
100	220 Å
1000	22 Å

There appears to be no reason why these transducers could not work to 1000 Gc. It is planned to investigate this type of transducer in conjunction with deformation potential devices for the microwave region.

4.7 Program for the Next Period. Although the general pattern of the ω-k diagram was computed for a particular set of parameters, the effect of varying any of the pertinent parameters will be studied before definite conclusions can be drawn from the plots. The significance of the complex ω and complex k will be further studied.

Spector's expressions for the acoustic gain (or attenuation) will be further evaluated for the deformation potential amplifier.

The design of the transducer mount will be completed and construction initiated. Initially copper, silver and gold films are to be studied in addition to the evaporated CdS film transducer.

DISTRIBUTION LIST

No. Copies	
2	Air Force Avionics Laboratory, Research and Technology Division, Attn: Captain P. W. Cary, Electronic Technology Division, Wright-Patterson Air Force Base, Ohio
2	Advisory Group on Electron Devices, Attn: Mr. Warren Kramer, 346 Broadway, 8th Floor, New York 13, New York
1	Commanding Officer, USAELRDL, Attn: SIGRA/SL-PRM, Mr. H. J. Hersh, Ft. Monmouth, New Jersey
1	Bureau of Ships, Attn: Mr. C. C. Walker, Code 681A1D, Washington 25, D. C.
1	Rome Air Development Center, RALTP, Attn: Mr. H. Chiosa, Griffiss Air Force Base, New York
1	Varian Associates, Central Research Laboratory, Attn: Dr. Herbert Kroemer, 611 Hansen Way, Palo Alto, California
1	Microwave Associates Inc., Attn: Dr. Arthur Uhlir, Jr., Burlington, Massachusetts
1	General Electric Company, Attn: E. L. Bartels, 118 West First Street, Dayton, Ohio 45402
1	Motorola Incorporated, Solid State Systems Division, Attn: Mr. N. G. Sakiotis, 3102 North 56th Street, Phoenix 10, Arizona
10	Commander, Defense Documentation Center, Cameron Station, Alexandria, Virginia
1	United Aircraft Research Labortory, Attn: Mr. A. W. Penney, Silver Lane, East Hartford, Connecticut
1	Texas Instruments Inc., Attn: Mr. Philip Thomas, P. O. Box 5012, Dallas, Texas
1	Microwave Electronics Corporation, Attn: Dr. Frank Olson, 3165 Porter Drive, Palo Alto, California
1	The University of Arizona, University Library, Tucson, Arizona
1	Electrical Engineering Department, Tulane University, Attn: Dr. Walter M. Nunn, Jr., New Orleans, Louisiana

No. Copies	
1	Naval Research Laboratories, Attn: Mr. Earle Ditzel, S212F, Washington, D. C.
1	Litton Industries, Emertron Information and Control Division, Antenna and Microwave Department, Attn: Mr. R. A. Sparks, 5009 Calvert Road, College Park, Maryland 20740
1	Office of Research Administration, Project Files, The University of Michigan, Ann Arbor, Michigan
15	Electron Physics Laboratory, The University of Michigan, Ann Arbor, Michigan

DD_____

The University of Michigan, Electron Physics Laboratory, Ann Arbor, Michigan, SOLID-STATE MICROWAVE RESEARCH, by D. C. Hanson, J. E. King, J. E. Rowe, C. Yeh. August, 1964, 52 pp. incl. illus. (Contract No. AF 33(657)-11587)

The characteristics of phonon interactions in solids are discussed in relation to possible parametric interactions in vanadium doped cadmium sulfide. The energy eigenvalues for cadium sulfide are plotted and discussed.

A theory of operation is proposed to explain the "Gunn effect" in bulk semiconductors. Experimental evidence is given for GaAs indicating radiation output in the wavelength region from 300-3000 microns.

The ω-β diagram for the longitudinal acoustic-wave amplifier is presented and discussed. The deformation potential acoustic-wave amplifier is analyzed. Thin film transducers are discussed.

UNCLASSIFIED

1. General Introduction
2. Phonon Interaction in Solids
3. Radiation from Solids
4. Traveling-Wave Phonon Interactions

I. Hanson, D. C
II. King, J. E.
III. Rowe, J. E.
IV. Yeh, C.

UNCLASSIFIED

DD_____

The University of Michigan, Electron Physics Laboratory, Ann Arbor, Michigan, SOLID-STATE MICROWAVE RESEARCH, by D. C. Hanson, J. E. King, J. E. Rowe, C. Yeh. August, 1964, 52 pp. incl. illus. (Contract No. AF 33(657)-11587)

The characteristics of phonon interactions in solids are discussed in relation to possible parametric interactions in vanadium doped cadmium sulfide. The energy eigenvalues for cadium sulfide are plotted and discussed.

A theory of operation is proposed to explain the "Gunn effect" in bulk semiconductors. Experimental evidence is given for GaAs indicating radiation output in the wavelength region from 300-3000 microns.

The ω-β diagram for the longitudinal acoustic-wave amplifier is presented and discussed. The deformation potential acoustic-wave amplifier is analyzed. Thin film transducers are discussed.

UNCLASSIFIED

1. General Introduction
2. Phonon Interaction in Solids
3. Radiation from Solids
4. Traveling-Wave Phonon Interactions

I. Hanson, D. C.
II. King, J. E.
III. Rowe, J. E.
IV. Yeh, C.

UNCLASSIFIED

DD_____

The University of Michigan, Electron Physics Laboratory, Ann Arbor, Michigan, SOLID-STATE MICROWAVE RESEARCH, by D. C. Hanson, J. E. King, J. E. Rowe, C. Yeh. August, 1964, 52 pp. incl. illus. (Contract No. AF 33(657)-11587)

The characteristics of phonon interactions in solids are discussed in relation to possible parametric interactions in vanadium doped cadmium sulfide. The energy eigenvalues for cadium sulfide are plotted and discussed.

A theory of operation is proposed to explain the "Gunn effect" in bulk semiconductors. Experimental evidence is given for GaAs indicating radiation output in the wavelength region from 300-3000 microns.

The ω-β diagram for the longitudinal acoustic-wave amplifier is presented and discussed. The deformation potential acoustic-wave amplifier is analyzed. Thin film transducers are discussed.

UNCLASSIFIED

1. General Introduction
2. Phonon Interaction in Solids
3. Radiation from Solids
4. Traveling-Wave Phonon Interactions

I. Hanson, D. C.
II. King, J. E.
III. Rowe, J. E.
IV. Yeh, C.

UNCLASSIFIED

DD_____

The University of Michigan, Electron Physics Laboratory, Ann Arbor, Michigan, SOLID-STATE MICROWAVE RESEARCH, by D. C. Hanson, J. E. King, J. E. Rowe, C. Yeh. August, 1964, 52 pp. incl. illus. (Contract No. AF 33(657)-11587)

The characteristics of phonon interactions in solids are discussed in relation to possible parametric interactions in vanadium doped cadmium sulfide. The energy eigenvalues for cadium sulfide are plotted and discussed.

A theory of operation is proposed to explain the "Gunn effect" in bulk semiconductors. Experimental evidence is given for GaAs indicating radiation output in the wavelength region from 300-3000 microns.

The ω-β diagram for the longitudinal acoustic-wave amplifier is presented and discussed. The deformation potential acoustic-wave amplifier is analyzed. Thin film transducers are discussed.

UNCLASSIFIED

1. General Introduction
2. Phonon Interaction in Solids
3. Radiation from Solids
4. Traveling-Wave Phonon Interactions

I. Hanson, D. C.
II. King, J. E.
III. Rowe, J. E.
IV. Yeh, C.

UNCLASSIFIED

DD_____

The University of Michigan, Electron Physics Laboratory, Ann Arbor, Michigan, SOLID-STATE MICROWAVE RESEARCH, by D. C. Hanson, J. E. King, J. E. Rowe, C. Yeh. August, 1964, 52 pp. incl. illus. (Contract No. AF 33(657)-11587)

The characteristics of phonon interactions in solids are discussed in relation to possible parametric interactions in vanadium doped cadmium sulfide. The energy eigenvalues for cadium sulfide are plotted and discussed.

A theory of operation is proposed to explain the "Gunn effect" in bulk semiconductors. Experimental evidence is given for GaAs indicating radiation output in the wavelength region from 300-3000 microns.

The ω-β diagram for the longitudinal acoustic-wave amplifier is presented and discussed. The deformation potential acoustic-wave amplifier is analyzed. Thin film transducers are discussed.

UNCLASSIFIED

1. General Introduction
2. Phonon Interaction in Solids
3. Radiation from Solids
4. Traveling-Wave Phonon Interactions

I. Hanson, D. C
II. King, J. E.
III. Rowe, J. E.
IV. Yeh, C.

UNCLASSIFIED

DD_____

The University of Michigan, Electron Physics Laboratory, Ann Arbor, Michigan, SOLID-STATE MICROWAVE RESEARCH, by D. C. Hanson, J. E. King, J. E. Rowe, C. Yeh. August, 1964, 52 pp. incl. illus. (Contract No. AF 33(657)-11587)

The characteristics of phonon interactions in solids are discussed in relation to possible parametric interactions in vanadium doped cadmium sulfide. The energy eigenvalues for cadium sulfide are plotted and discussed.

A theory of operation is proposed to explain the "Gunn effect" in bulk semiconductors. Experimental evidence is given for GaAs indicating radiation output in the wavelength region from 300-3000 microns.

The ω-β diagram for the longitudinal acoustic-wave amplifier is presented and discussed. The deformation potential acoustic-wave amplifier is analyzed. Thin film transducers are discussed.

UNCLASSIFIED

1. General Introduction
2. Phonon Interaction in Solids
3. Radiation from Solids
4. Traveling-Wave Phonon Interactions

I. Hanson, D. C.
II. King, J. E.
III. Rowe, J. E.
IV. Yeh, C.

UNCLASSIFIED

DD_____

The University of Michigan, Electron Physics Laboratory, Ann Arbor, Michigan, SOLID-STATE MICROWAVE RESEARCH, by D. C. Hanson, J. E. King, J. E. Rowe, C. Yeh. August, 1964, 52 pp. incl. illus. (Contract No. AF 33(657)-11587)

The characteristics of phonon interactions in solids are discussed in relation to possible parametric interactions in vanadium doped cadmium sulfide. The energy eigenvalues for cadium sulfide are plotted and discussed.

A theory of operation is proposed to explain the "Gunn effect" in bulk semiconductors. Experimental evidence is given for GaAs indicating radiation output in the wavelength region from 300-3000 microns.

The ω-β diagram for the longitudinal acoustic-wave amplifier is presented and discussed. The deformation potential acoustic-wave amplifier is analyzed. Thin film transducers are discussed.

UNCLASSIFIED

1. General Introduction
2. Phonon Interaction in Solids
3. Radiation from Solids
4. Traveling-Wave Phonon Interactions

I. Hanson, D. C.
II. King, J. E.
III. Rowe, J. E.
IV. Yeh, C.

UNCLASSIFIED

DD_____

The University of Michigan, Electron Physics Laboratory, Ann Arbor, Michigan, SOLID-STATE MICROWAVE RESEARCH, by D. C. Hanson, J. E. King, J. E. Rowe, C. Yeh. August, 1964, 52 pp. incl. illus. (Contract No. AF 33(657)-11587)

The characteristics of phonon interactions in solids are discussed in relation to possible parametric interactions in vanadium doped cadmium sulfide. The energy eigenvalues for cadium sulfide are plotted and discussed.

A theory of operation is proposed to explain the "Gunn effect" in bulk semiconductors. Experimental evidence is given for GaAs indicating radiation output in the wavelength region from 300-3000 microns.

The ω-β diagram for the longitudinal acoustic-wave amplifier is presented and discussed. The deformation potential acoustic-wave amplifier is analyzed. Thin film transducers are discussed.

UNCLASSIFIED

1. General Introduction
2. Phonon Interaction in Solids
3. Radiation from Solids
4. Traveling-Wave Phonon Interactions

I. Hanson, D. C.
II. King, J. E.
III. Rowe, J. E.
IV. Yeh, C.

UNCLASSIFIED